# Rational Preparation of Well-Defined Multinuclear Iridium-Aluminum Polyhydride Clusters and Comparative Reactivity

Leon Escomel, Naime Soule, Emmanuel Robin, Iker del Rosal, Laurent Maron, Erwann Jeanneau, Chloé Thieuleux, Clément Camp

# Rational Preparation of Well-Defined Multinuclear Iridium-Aluminium Polyhydride Clusters and Comparative Reactivity

Léon Escomel,[a] Naïme Soulé,[a] Emmanuel Robin,[a] Iker Del Rosal,[b] Laurent Maron,[b] Erwann Jeanneau,[c] Chloé Thieuleux[a] and Clément Camp*[a]

[a] Laboratory of Catalysis, Polymerization, Processes and Materials, CP2M UMR 5128, CNRS, Université de Lyon, Institut de Chimie de Lyon, Université Lyon 1, ESCPE Lyon, 43 Bd du 11 Novembre 1918, F-69616 Villeurbanne, France.

[b] Université de Toulouse, CNRS, INSA, UPS, UMR 5215, LPCNO, 135 Avenue de Rangueil, F-31077 Toulouse, France.

[c] Université de Lyon, Centre de Diffractométrie Henri Longchambon, 5 Rue de la Doua, 69100 Villeurbanne, France.

**ABSTRACT:** We report an original alkane elimination approach, entailing the protonolysis of triisobutylaluminium by the acidic hydrides from $Cp^*IrH_4$. This strategy allows access to a series of well-defined tri- and tetranuclear iridium aluminium polyhydride clusters, depending on the stoichiometry: $[Cp^*IrH_3Al(i\text{Bu})_2]_2$ (**1**), $[Cp^*IrH_2Al(i\text{Bu})]_2$ (**2**), $[(Cp^*IrH_3)_2Al(i\text{Bu})]$ (**3**) and $[(Cp^*IrH_3)_3Al]$ (**4**). Contrary to most transition metal aluminohydride complexes which can be considered as $[AlH_{x+3}]^{x-}$ aluminates and $LnM^+$ moieties, the situation here is reversed: these complexes have original structures which are best described as $[Cp^*IrH_x]^{n-}$ iridate units surrounding cationic Al(III) fragments. This is corroborated by reactivity studies, which show that the hydrides are always retained at the iridium sites and that the $[Cp^*IrH_3]^-$ moieties are labile and can be transmetallated to yield potassium ($[KIrCp^*H_3]$, **8**) or silver ($([AgIrCp^*H_3]_n$, **10**) derivatives of potential synthetic interest. DFT calculations show that the bonding situation can vary in these systems, from 3-centre 2-electron hydride-bridged Lewis adducts of the form Ir–H→Al, to direct polarized metal–metal interaction from donation of *d*-electrons of Ir to the Al metal, and both types of interactions are at place to some extent in each of these clusters.

## INTRODUCTION

Metal hydride clusters are fascinating molecular objects which are attracting increasing interest as potential hydrogen storage materials,[1–4] or for their ability to promote unusual small molecules activations[5–11] and catalytic transformations[12–14] through original pathways. The vast majority of polynuclear metal hydride derivatives synthesized to date are homometallic assemblies. Yet combining two metallic elements in polyhydride clusters is appealing in order to combine and reach unusual structures and properties. Although attractive examples of heterobimetallic polyhydrides were described,[15–22] the main limitation of this field to expand is rational synthesis. In most cases, polyhydride transition metal clusters are formed through hydrogenolysis of organometallic precursors with $H_2$, silanes or boranes.[6,7,13,23,24] However, it is very difficult to selectively control the nuclearity, composition and topology of the resulting polyhydride clusters since complex phenomena typically occur in the course of these syntheses (eg. redistribution, rearrangement or segregation phenomena), often leading to unpredictable mixtures of compounds. These considerations are even more dramatic when two different metal precursors are engaged, rendering the rational preparation of heterobimetallic entities extremely challenging. Post-modification strategies, such as doping of monometallic clusters with heterometal atoms,[25–30] or rearrangement of two independently synthesized monometallic clusters,[31–33] are emerging approaches that have attracted substantial interest recently, but so far limited to thiolate or carbonyl metal clusters. Lability phenomena and metal exchange strategies in polyhydride metal clusters is much less investigated to date.

The reaction of acidic metal hydrides with nucleophilic metal alkyl derivatives, known as alkane elimination reaction, is an efficient way to prepare metal-metal bonded species.[34–41] In the case where polyhydrides are reacted with polyalkyls, succeeding alkane eliminations can occur, opening a way to the synthesis of polynuclear heterobimetallic species assembled through metal-metal bonds and/or bridging hydride ligands. We have recently reported the reactivity of $Cp^*IrH_4$ with a tantalum neopentyl/neopentylidene derivative (Scheme 1-top),[42–44] and have shown that double alkane elimination occurs, leading to a trinuclear TaIr2 pentahydride complex (Scheme 1). Given the increasing surge of interest for compounds associating aluminium with *d*-block metals,[45–60] and featuring original chemistry, we turned our attention to the preparation of aluminium-iridium compounds using the same alkane elimination route. We notably described recently the preparation of polarized $Al(III)^{\delta+}$–$Ir(III)^{\delta-}$ dinuclear species (Scheme 1) able to promote the cooperative reductive cleavage of heteroallenes ($CO_2$, AdNCO).[60] In that case, the steric hindrance provided by a bulky aryloxide ligand implemented on the Al center prevents subsequent alkane elimination. However, pioneering work by Bergman and coworkers have demonstrated the possibility of double deprotonation of a iridium(III) dihydride complex by the sterically unhindered triethylaluminium reagent, affording a

unique $Ir_2Al_2$ tetranuclear species (Scheme 1) which structure and reactivity was not explored in details.[61] Inspired by this early achievement from Bergman, and in continuation of our work, we report herein the controlled preparation of a series of well-defined tri- and tetra-nuclear iridium aluminium polyhydride species based on a stepwise alkane elimination strategy, and explore their reactivity.

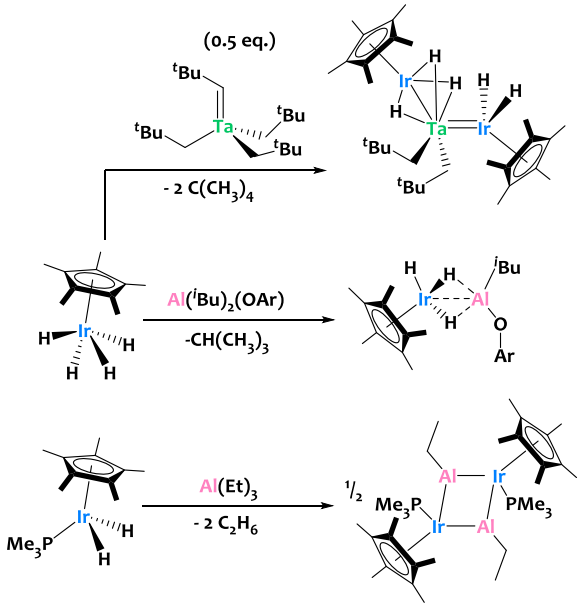


**Scheme 1. Representative reductive alkane elimination reactivity of pentamethyl-cyclopentadienyl iridium polyhydrides with nucleophilic metal-alkyl derivatives reported in the literature.**[42,60,61]

## RESULTS AND DISCUSSION

### Stepwise preparation and molecular structure of well-defined multinuclear iridium/aluminium polyhydride clusters

Treatment of $IrCp^*H_4$ with one equivalent of triisobutylaluminium in pentane at room temperature leads to the formation of the tetranuclear complex $[Cp^*IrH_3Al(iBu)_2]_2$, **1**, with evolution of one equivalent of isobutane *per* aluminium site as quantified by $^1$H-NMR (Scheme 2). The identity of **1** was first scrutinized by $^1$H-NMR in $C_6D_6$ solution (see Figure S1). In the alkyl region, the spectrum displays one Cp* signal at δ = 1.94 ppm integrating for 15H *per* iridium center, in agreement with 1 Cp* ligand *per* Ir site. The resonances relating to the isobutyl groups showcase a stoichiometry of 2 isobutyl fragments *per* aluminium center and the hydride signal appears as a singlet at δ = -16.54 ppm integrating for 3H *per* Ir site. Yellow block-shaped single crystals of **1** were isolated upon cold (-40°C) crystallization of the reactional mixture after 2 hours of reaction.

The crystal structure of **1**, determined by X-Ray diffraction, is shown on Figure 1-top. The first noticeable feature of this structure is the centrosymmetric $\{Ir_2Al_2\}$ core. This tetranuclear diamond-shape core is perfectly planar, with Ir-Al-Ir angles of 101.18(6)° and Al-Ir-Al angles of 78.82(6)°. The geometry around the aluminium centers is pseudo-tetrahedral ($C_{iBu}$-Al-$C_{iBu}$ angles = 119.0(3)°, $C_{iBu}$-Al-Ir angles in the range 103.90(19)°-114.93°). The Ir-Al distances (averaged at 2.72(1) Å) are longer than those reported in the rare examples of unsupported Ir-Al bonds (2.45-2.51 Å),[61,62] and the average formal shortness ratio (r=1.085)[63,64] is above unity. Therefore, the close proximity between the Al and Ir centers in **1** is most likely the result of the presence of bridging hydrides. Even if the hydrides could not be located in the XRD Fourier Map, hint of the presence of terminal hydrides can be given in these series of complexes by the tilting of the Cp* ligands. To evaluate this distortion, we propose a new descriptor, α = ½(θ+θ') (see Figure 2), which measures the difference in the two angles between the Cp*centroids, the iridium centers and the centroid of the $Ir_2Al_2$ core. In the case of **1**, α = 163.7(1)°, indicating a moderate twisting of the Cp* rings. This suggests that at least some of the hydrides are on terminal position on the Ir sites. For instance, in $[Cp^*Ir(\mu\text{-}H_3)RuCp^*]$,[65] featuring 3 bridging hydrides, the two Cp* rings are almost parallel (α = 178.2); while in $[Cp^*Ru(\mu\text{-}H_3)WH_3Cp^*]$,[66] featuring 3 bridging hydrides and 3 terminal hydrides, a tilting of the Cp* is observed (α = 158.7°). Our group also reported a related iridium-tantalum complex, $[IrHCp^*Ta(Np)_2]_2$,[42] featuring a similar α angle of 160.1°. In this complex, the hydrides were located in terminal position on the Ir sites. The tilting of the Cp* ligands thus suggests that there is at least a terminal hydride per Ir, yet there seems to be no correlation between the number of terminal hydrides and that distortion, nor the presence or absence of bridging hydrides.

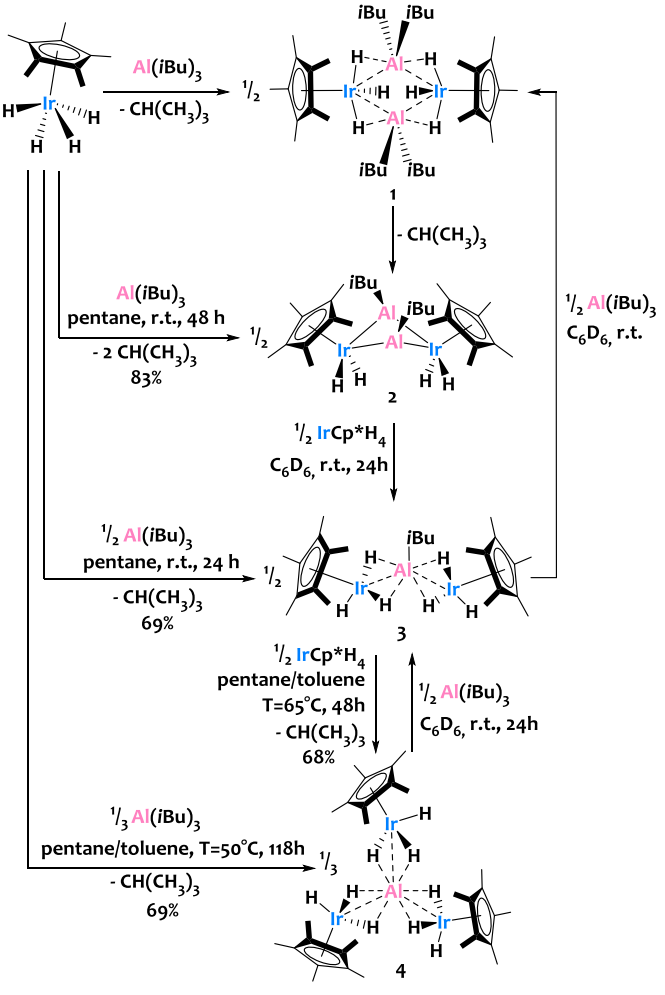

**Scheme 2. Synthesis of the Al-Ir tetrametallic and trimetallic species 1-4.**

We thus conducted DFT calculations, and in the most stable computed structure, which reproduces very well all the geometrical parameters of the crystallographic structure (see details below), one terminal hydride is found *per* iridium center, along with four bridging Ir-H-Al hydrides (two per iridium center), as represented on Scheme 2.[42] Note that these considerations and proposed hydride topology is only relevant in the solid state. Fluxional behaviour with rapid exchange between the hydrides positions is occurring in solution, as frequently found in metal-polyhydride compounds,[43,44,60,67] since only one hydride signal integrating for 3H *per* Ir is found in the $^1$H NMR spectrum of **1**.

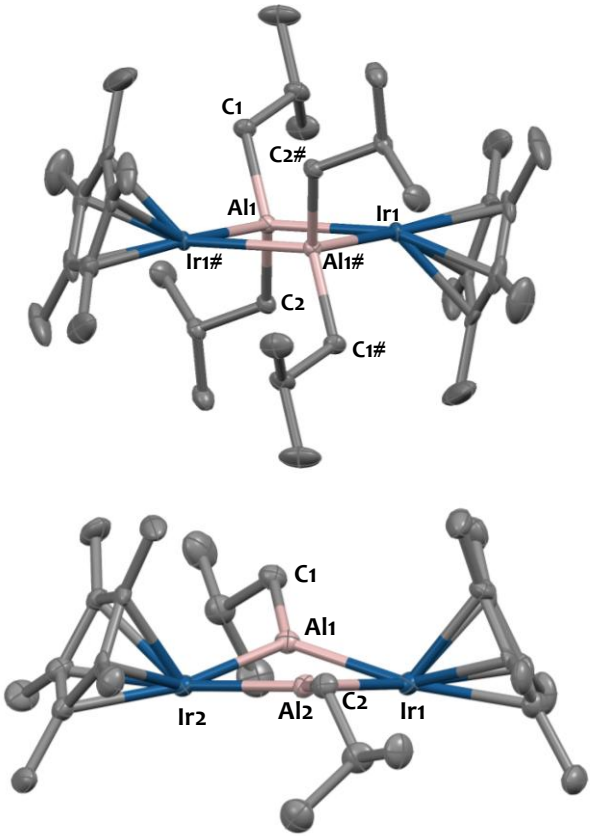


**Figure 1**. Solid-state molecular structures of **1** (top) and **2** (bottom). Ellipsoids are represented with 30% probability. Hydrogen atoms have been omitted for clarity. Selected bond distances (Å) and angles (°) for **1**: Ir1-Al1 2.734(2), Ir1#-Al1# 2.720(2), Al1-C2 1.998(6), Al1-C1 2.008(6), Ir1-Al1-Ir1# 101.18(6), Al1-Ir1-Al1# 78.82(6), (Ir1#-Al#1-Ir1-Al1)$_{centroid}$-Ir-Cp*$_{centroid}$ 163.77. For **2**: Ir1-Al1 2.449(6), Ir1-Al2 2.438(6), Al1-Al2 2.582(8), Al1-C1 1.96(2), Al2-C2 1.987(19). Ir2-Al1-Ir1 112.5(2), Ir2-Al2-Ir1 113.4(2) Al2-Ir1-Al1 63.80(18), C1-Al1-Ir1 125.3(7), C1-Al1-Ir2 122.2(7), C5-Al2-Ir1 119.6(6), C5-Al2-Ir2 126.9(6), (Ir1-Al1-Ir2-Al2)$_{centroid}$-Ir1-Cp*$_{centroid}$ 151.78, (Ir1-Al1-Ir2-Al2)$_{centroid}$-Ir2-Cp*$_{centroid}$ 151.21.

Complex **1** is unstable in $C_6D_6$ solution at room temperature and evolves within a few hours to form the stable complex $[Cp^*IrH_2Al(i\text{Bu})]_2$, **2** (Scheme 2), through the loss of one additional isobutyl fragment *per* Al, which is released as isobutane. After two days of reaction at room temperature, complex **2** is isolated in 83% yield. The molecular structure of **2** is confirmed by multi-nuclei ($^1$H, $^{13}$C) solution NMR and infrared (IR) spectroscopies, elemental analysis and X-ray diffraction studies. The $^1$H-NMR spectrum of **2** (recorded in $C_6D_6$) shows a very high field hydride resonance emerging as a singlet at δ = -16.68 ppm and integrating for 4H. The infrared spectrum of **2** exhibits a strong stretching vibrational mode at σ = 1989.4 cm$^{-1}$ typical of a terminal Ir-H stretch.[42] Yellow plate-shaped single-crystals of **2** suitable for X-ray diffraction analysis were grown in a cold (-40°C) and saturated pentane solution of **2**. The solid-state molecular structure of **2** (Figure 1, bottom) displays unusual structural features. Contrary to **1** and to the related $[Cp^*IrPMe_3AlEt]_2$ complex reported by Bergman,[61] the tetranuclear $\{Ir_2Al_2\}$ core in **2** is not centrosymmetric nor planar, but adopts a saddle topology with the two Al centers lying slightly above the two Ir centers (mean deviation from plane = 0.19(2) Å). The Ir-Al distances lie in the range 2.426(6) - 2.449(6) Å, which is considerably shorter than in **1** (2.72(1) Å) and in the range of the rare unsupported Ir-Al bonds (2.45-2.51 Å).[61,62] The formal shortness ratio (r = 0.972)[63,64] is slightly below unity suggesting some degree of metal-metal interactions between the Ir and the Al sites. The Ir-Al-Ir angles in **2** (112.5(2)° and 113.4(2)°) are considerably more obtuse than in **1** (101.18(6)°) to favor trigonal planar geometries at the Al sites, which are located only within 0.01(1)Å of the Ir1-Ir2-C1 or Ir1-Ir2-C2 planes. As a result, the Al-Ir-Al angles in **2** (63.8(2)° and 64.1(2)°) are much smaller than in **1** (78.82(6)°). This peculiar geometric arrangement results in an unexpected very short Al-Al distance of 2.582(8) Å. This Al-Al separation is remarkably short when compared to reported Al-Al single bonds: the Al-Al distance in $[Cp^*Al]_4$ is 2.77 Å[68] and Al-Al single bond distances in dinuclear Al-Al species lie in the range [2.53-2.70 Å].[69–75] However, our DFT calculations (see below) suggest that compound **2** is best described as containing two Al(III) cations with little to no Al-Al bonding despite their close proximity. The twisting of the Cp* rings with respect to the $Ir_2Al_2$ core is more pronounced in **2** (α = 151.5(1)°) than in **1** (α = 163.7(1)°), as a result of the presence of two hydrides in terminal position on each Ir center, as supported by DFT calculations (see below).

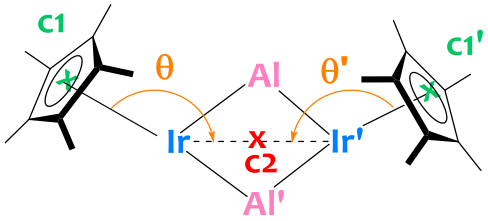


**Figure 2**. Definition of a new metrical parameter α = (θ+θ')/2 characteristic of iridium-hydride locations (terminal or bridging).

In summary, the acidic hydrides from $Cp^*IrH_4$ promote the protonolysis of Al-isobutyl groups, leading to $[Cp^*IrH_3]^-$ moieties which then act as proton sources to cleave another Al-isobutyl group, resulting in formally doubly deprotonated $[Cp^*IrH_2]^{2-}$ fragments, which are bridged by $Al(i\text{Bu})^{2+}$ units in cluster **2**. Note that the deprotonation of Ir-H with strong bases leading to highly reactive iridate species was described in some occurrences,[62,76–81] while the double deprotonation

of an iridium dihydride by metal alkyl reagents is much more rare, and was only observed by us (M = Ta)[42] and Bergman (M = Al).[61] (Scheme 1).

In order to better understand the alkane elimination sequence in these systems and access clusters of various nuclearities and compositions, we studied the reaction of triisobutylaluminium with an excess of $IrCp^*H_4$. Treatment of $Al(iBu)_3$ with 2 equivalents of $IrCp^*H_4$ in pentane leads to the formation of the trinuclear $[Ir((Cp^*)(H)(\mu\text{-}H_2))_2Al(iBu)]$ complex **3** in 69% yield as a light yellow powder (Scheme 2). Single-crystals of **3** suitable for XRD analysis were grown in a cold (-40°C) saturated solution of **3** in pentane. The solid-state structure of **3**, shown on Figure 3 (top), settles the trinuclear nature of the complex where two $[Cp^*IrH_3]^-$ fragments are bridged by an $Al(iBu)^{2+}$ motif. The aluminium center adopts a pseudo trigonal planar geometry with angles lying in the 115-126° range. The averaged Al-Ir distances of 2.435(6) Å in **3** are in the same range than those in complex **2**. The $^1$H-NMR spectrum of **3**, recorded in $C_6D_6$ solution (Figure S6), shows a hydride signal at δ = -16.64 ppm integrating for 6H, two IrCp*fragments (δ = +2.03 ppm integrating for 30H) and one Al(*i*Bu) pattern ($\delta_{CH}$ = 2.49 ppm, 1H; $\delta_{CH3}$ = 1.29 ppm, 6H; $\delta_{CH2}$ = 0.56 ppm, 2H) in agreement with the proposed molecular structure for **3**. The Diffuse Reflectance Infrared Fourier Transform (DRIFT) spectrum of **3** (Figure S48) displays two intense M-H vibrators at σ = 2151 $cm^{-1}$ and 2014 $cm^{-1}$ suggesting two types of hydrides environments. This assumption is further supported by the observed tilting of Cp* rings with respect of the Ir-Al axes in the solid-state structure of **3** (Figure 3-top), with Al-Ir-$Cp^*_{centroid}$ angles averaged at 140.7(2)°, probably imparted by the presence of a terminal hydride, also supported by DFT calculations (see SI). Note that Stephan and co-workers reported in 1998 a zirconium-aluminium complex, $[(Cp')_2ZrH(\mu\text{-}H)_2]_2AlH$ (Cp' = $Me_3SiC_5H_4$), structurally related to the present species, but prepared through salt metathesis.[82] Complex **3** is stable even upon heating to 60°C. It is still unclear why the elimination of the remaining isobutyl ligand is not observed here, while **1** is quickly converted into **2** through internal isobutyl protonolysis.

Quite interestingly, the reaction of complex **2** with 2 equivalents of $IrCp^*H_4$ leads also to product **3** quantitatively (see Figure S9). This reaction is quite informative regarding the processes at place in these systems. Here, $Cp^*IrH_4$ acts as a Brønsted acid, but the proton transfer preferentially occurs at the Ir sites from **2**, rather than at the isobutyl aluminium groups, as confirmed by the absence of isobutane elimination. This testify to the strong basicity of the $[Cp^*IrH_2]^{2-}$ fragment. This reaction also advocates for some degree of lability in these systems, since the di-aluminium derivative **2** is converted into a mono-aluminium species, **3**, as a result of iridate ligands redistribution. This motivated us to investigate the reaction of **3** with 0.5 equivalent of $Al(iBu)_3$. NMR reaction monitoring shows that after two hours at room temperature, compound **3** is quantitatively converted into **1**, as a result of isobutyl / iridate ligands redistribution (Scheme 2). Complex **1** is then slowly evolving into **2** through isobutane elimination, as expected (see Figure S10). This confirms that these assemblies are labile, leading to metal/ligand redistribution phenomena, which are faster than the protonolysis reactivity in the present case. This paves the way towards the preparation of more diverse architectures through metal substitution.

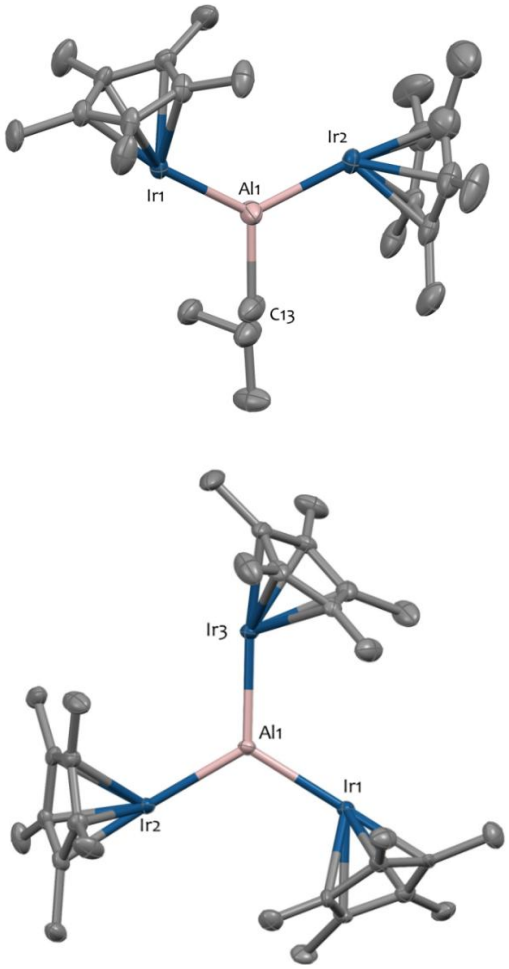


**Figure 3.** Solid-state molecular structures of **3** (top) and **4** (bottom). Ellipsoids are represented with 30% probability. Hydrogen atoms have been omitted for clarity. Two independent molecules were found in the asymmetric unit of **4** (Z'=2) but one of them has been omitted for clarity. Selected bond distances (Å) and angles (°) for **3**: Ir1-Al1 2.437(6), Ir2-Al1 2.432(6), Al1-C13 2.04(3), Ir2-Al1-Ir1 125.4(3), C13-Al1-Ir1 116.4(10), C13-Al1-Ir2 115.7(10), Al1-Ir1-$Cp^*_{centroid}$ 140.20, Al1-Ir2-$Cp^*_{centroid}$ 141.24. For **4** (average values between both molecules found in the asymmetric unit): Ir1-Al1 2.477(8), Ir2-Al1 2.475(3), Ir3-Al1 2.484(8). Ir1-Al1-Ir2 118.57(62) Ir1-Al1-Ir3 120.14(62), Ir2-Al1-Ir3 121.13(62), Al1-Ir1-$Cp^*_{centroid}$ 139.26, Al1-Ir2-$Cp^*_{centroid}$ 140.25, Al1-Ir3-$Cp^*_{centroid}$ 142.22.

Finally, the total dealkylation - *i.e.* triple isobutane elimination - is achieved upon treatment of $Al(iBu)_3$ with 3 equivalents of $IrCp^*H_4$ in a hot toluene/pentane solution (50°C) for one week. This procedure leads to the formation of the tetranuclear cluster $[\{Cp^*Ir(H)(\mu\text{-}H_2)\}_3Al]$, **4**, isolated as colorless block-shaped crystals after cold recrystallization in pentane (69 % yield). Interestingly, we noticed by $^1$H NMR reaction monitoring that species **3** is formed in the course of the reaction as an intermediate. We thus examined the preparation of complex **4** by mixing stoichiometric amounts of **3** and $IrCp^*H_4$ in a hot toluene/pentane solution (65°C) for 2 days (Scheme 2). The full dealkylation is proved by the absence of isobutyl signals in the $^1$H and $^{13}$C-NMR spectra,

which only display Ir-Cp* ($\delta_{1H}$ = 2.11 ppm, $\delta_{13C}$ = 93.62 & 11.26 ppm) and Ir-H resonances ($\delta_{1H}$ = -16.38 ppm). The solid-state structure of **4**, obtained by XRD crystallography, is shown on Figure 3-bottom. Complex **4** adopts a propeller-like C3-symmetric structure where three $[Cp^*IrH_3]^-$ moieties are ligated to an $Al^{3+}$ center. The Al-Ir distances are ranging from 2.475(3) Å to 2.484(8) Å. These intermetallic distances are slightly elongated in comparison to those in **3** (2.435(6) Å on average) but still remain much shorter than those in **1** (2.72(1) Å), and are compatible with direct Ir-Al interactions. The pronounced tilting of the three Cp* rings (Cp*centroid-Ir-Al angles in the range 139- 142°) suggests the presence of terminal hydrides onto the iridium sites, as for complex **3**. The DRIFT spectrum of **4** is very similar to that of **3**, which also supports the presence of two types of hydrides environments in the solid state. The geometry of complex **4** optimized by DFT (shown on Figure 5 below) is in excellent agreement with the experimental X-ray single crystal structure, and contains one terminal Ir–H hydride *per* Ir site, and 6 hydrides bridging the central $Al^{3+}$ site in a trigonal prismatic arrangement. Note that in solution the hydrides are highly fluxional, since a single averaged hydride signal integrating for 3H per iridium center is observed by $^1$H NMR spectroscopy, even at -50°C (see Figure S12).

To complete this reaction sequence, we studied the reaction of Al(*i*Bu)$_3$ with two equivalents of complex **4**. This leads to the quantitative formation of complex **3**, as a result of scrambling of the alkyl and iridate moieties surrounding the Al sites. Ultimately, this well-behaved protonolysis and ligand-exchange reaction sequence allows the controlled preparation of Al/Ir clusters of various compositions and topologies. The isolation of **4** is a nice achievement in view of the synthetic challenges associated to the stabilization an Al(III) center surrounded only by transition metal hydride fragments. To the best of our knowledge, only four examples describing $[M_3Al]$ (M = Ru or Zr) polyhydride molecular edifices, represented on Figure 4, are known.[19,21,22,82]

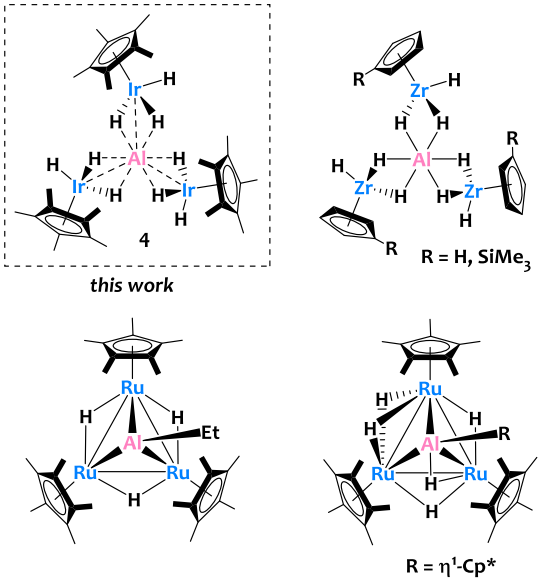


**Figure 4**. $M_3Al$ tetranuclear polyhydrides (M = Zr,[21,82] Ru,[19,22] Ir) described to date.

We also explored the reactivity of $Cp^*IrH_4$ with two equivalents of Al(*i*Bu)$_3$. This leads to the elimination of isobutene an to the formation of an intricate mixture of Ir-H species that we were, unfortunately, unable to separate and unambiguously attribute (Figure S17).

Binary hydride materials, such as $Li_3AlH_6$, consisting of $[AlH_6]^{3-}$ octahedra surrounded by three $Li^+$ cations, are also known, and have attracted appreciable attention as potential hydrogen storage material. The bonding situation in $Li_3AlH_6$ consists in strong covalent bonding between Al and the hydrides and weaker ionic bonding between the aluminate $[AlH_6]^{3-}$ units and the $Li^+$ cations.[83,84] This bonding situation appears opposite to that observed in compounds **1-4**, in which the hydrides seem to interact much strongly with the Ir sites, to form iridate units held together by cationic Al(III) moieties. To get deeper insights into the structure and bonding in these systems, and help deciphering the metal-hydride and metal-metal interactions, DFT calculations (B3PW91) were carried out (see ESI for complete computational details). For complex **1**, only one stable structure was obtained, despite a large exploration of possible conformers. The optimized tetranuclear diamond-shape geometry is in good agreement with the solid state molecular structure of **1** (e.g. Ir-Al-Ir angles of 100.5°, Al-Ir-Al angles of 79.5° and averaged Ir-Al distances of 2.75 Å, see Figure S57). The moderate twisting (α = 163.8°) of the Cp* rings is also reproduced computationally. Regarding the hydride positions, as aforementioned, one terminal hydride, labeled as H(η), is found *per* iridium center, along with four bridging hydrides, called H(μ), Ir-H→Al (two per iridium center). Natural bonding orbital (NBO) analyses of **1** clearly indicate, for each Ir atom, the presence of three covalent Ir–H interactions (with 47–56% contribution from the Ir *spd* hybrid orbital). At the second-order donor-acceptor level, donations from the Ir–H(μ) bonds into the Al empty *sp* orbital are observed, in line with the presence of three-center–two-electron (3c-2e) Ir–H(μ)→Al bonds. The presence of a covalent bond between Ir and H(μ) is also corroborated by the calculated Ir–H(μ) Wiberg bond indexes (WBIs, Figure 5) of 0.66. Al – H(μ) WBIs of 0.13 are found, in line with electron delocalization from the Ir–H(μ) bonds onto acceptor orbitals on Al atoms. Interestingly, a similar donation is obtained from the Ir–H(η) bonds into the Al empty *sp* orbital of each Al atom as well as similar calculated WBIs of 0.08 between these H(η) atoms and each Al atom. These calculations suggest a pseudo-face capping character of these terminal hydrides in agreement with the experimentally observed fluxional behaviour leading to the exchange between the hydride positions. Natural charges in **1** were calculated as −0.958 on Ir and +1.776 on Al, with a calculated Ir–Al WBIs of 0.2 indicating the presence of a slightly bonding interaction between Ir and Al (donation from a Ir *d* lone pair into the Al empty *sp* orbital). These analyses also show the absence of any Al-Al bonding interaction in complex **1** (Al - Al WBI of 0.03). For complex **2**, a conformational analysis has revealed four possible conformers in an energy range of only 14.0 kcal.mol$^{-1}$ (see Figure S58). The most stable structure exhibits two hydrides in terminal position on each Ir center while the structure with two terminal hydrides and two brdiging Ir-H→Al hydrides is less stable by 6.5 kcal.mol$^{-1}$. Finally, two other conformers with four bridging hydrides Ir-H→Al were also obtained, but are the least

stable (10.6 and 14.0 kcal.mol$^{-1}$ above the lowest energy structure). Interestingly enough, only the most stable structure exhibits an Ir-H stretching vibrational mode in between 1977 and 2011 cm$^{-1}$ in agreement with the IR data.

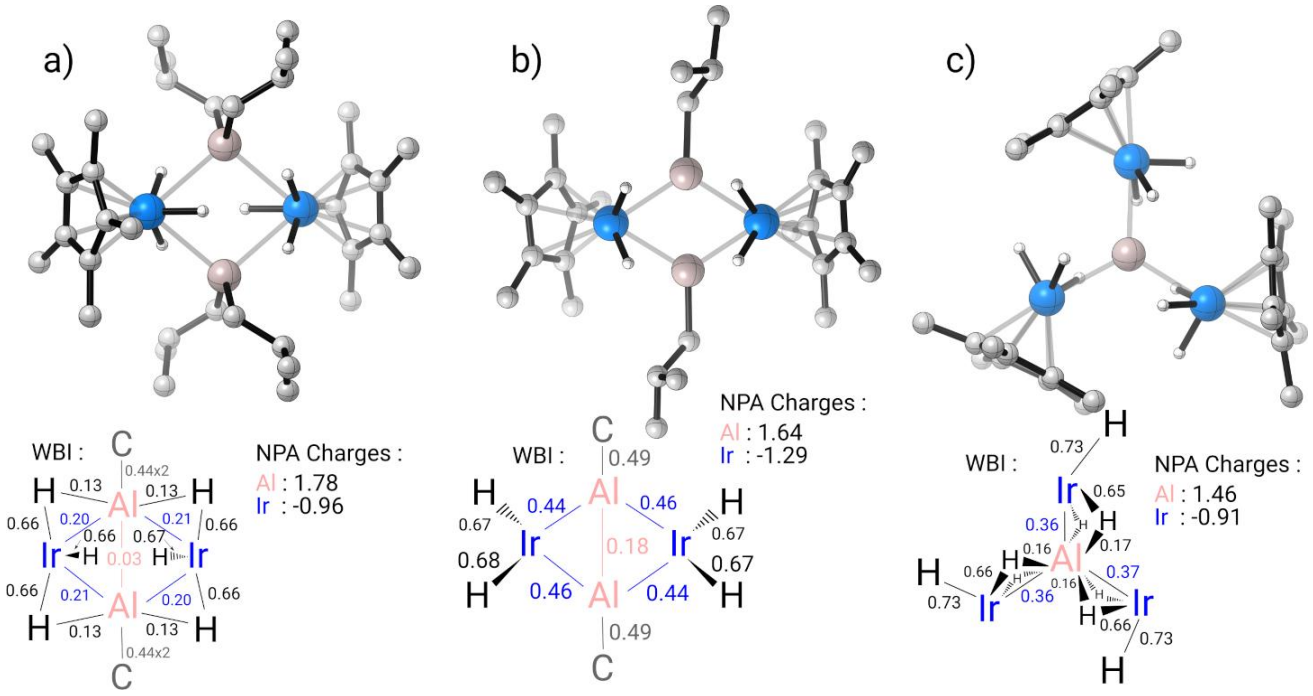


**Figure 5.** Most stable computed structures, NPA charges and Wiberg bond indexes of complexes **1**, **2** and **4**.

Finally, a good correlation between the crystallographic and the calculated structure of the most stable conformer is found (see Figure S57) : (*i*) as experimentally observed this complex adopts a saddle topology; (*ii*) the calculated Ir-Al distances lie in the range 2.449 - 2.465 Å and the short Al-Al distance is equal to 2.643 Å; (*iii*) the Ir-Al-Ir, Al-Ir-Al and α angles are equal to, respectively, 113.5°, 65.0° and 154.3°. In this case, as for complex **1**, the NBO analyses and the calculated WBIs clearly indicate the presence of a covalent bond between Ir and H as well as an electron delocalization from these bonds onto acceptor orbitals on Al atoms. However, as aforementioned, these calculations confirmed that no Al-Al bond is present in complex **2** even though the Al-Al WBI in complex **2** is higher than in complex **1** (0.18 *vs.* 0.03). The tetranuclear complex **4** has also been theoretically studied. In this case, as for complex **1**, the conformational analysis leads to only one stable structure (see Figure 5). The optimized geometry indicates that six Ir-H-Al bridging hydrides are arranged around the central Al atom in a trigonal prismatic geometry as well as the presence of one terminal Ir–H hydride *per* Ir site. The optimized structure is in excellent agreement with the experimental one with Al-Ir distances around 2.486 Å and an α angle of 140.8° (see Figure S57). The Al-Ir WBIs in complex **4** are slightly smaller (0.36) than in complex **2** (0.44) but higher than in complex **1** (0.20), in agreement with the observed variation of the intermetallic distances. For complex **4**, as for **1** and **2**, the Ir-H WBIs are around 0.65 for bridging hydrides and 0.73 for terminal hydrides, in line with mainly covalent interaction. The Al-H WBIs are around 0.17 in line with electron delocalization from the Ir-H bond onto an acceptor orbital on Al. The Natural Population Analysis (NPA) charge on iridium and aluminium are slightly smaller than in complexes **1** and **2**, taking values between -0,904 and -0.910 for Iridium and +1.463 for aluminum.

### Comparative reactivity

The main reactivity trends of the two archetypal clusters of this series, **2** and **4**, were then investigated.

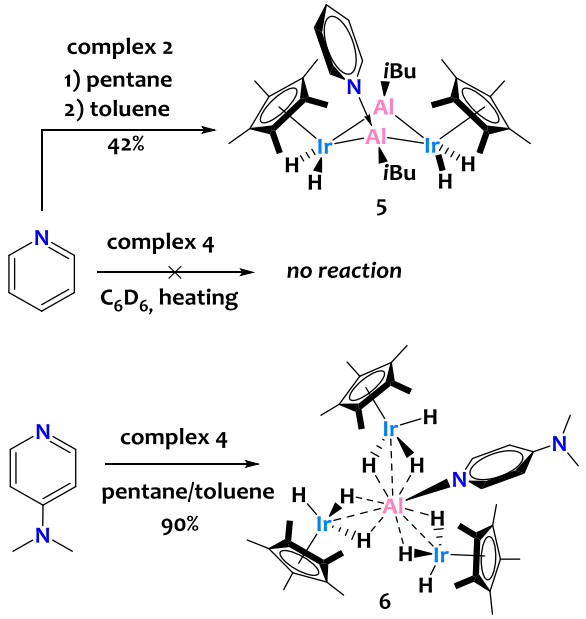


**Scheme 4. Reactivity of the Al-Ir heterobimetallic complexes 2 and 4 towards pyridine derivatives.**

In view of understanding the behavior of compounds **2** and **4** towards donor ligands, we first studied their reactivity with pyridine. Treatment of **2** with 1 equivalent of pyridine

leads to the pyridine mono-adduct **5** (Scheme 4). When excess amounts of pyridine are added onto **2**, several species are observed by $^1$H NMR spectroscopy monitoring of the solution, most likely corresponding to poly-pyridine adducts, yet upon drying *in vacuo* the mono-adduct **5** is obtained quantitatively. Isolation of **5** as a pure dark orange crystalline material was performed by a cold recrystallization of the crude solid in the minimum amount of toluene. The $^1$H-NMR spectrum of **5**, recorded in $C_6D_6$ solution, features shifted pyridine signals at δ = 8.72, 6.81 and 6.55 ppm indicating its coordination to Al in solution. The DRIFT spectral signature of **5** is similar to that of **2**, with appearance of a new ν Ir-H band at σ = 2110 cm$^{-1}$, which is assigned to an asymmetric stretching mode as a result of desymmetrization of the complex upon pyridine ligation.

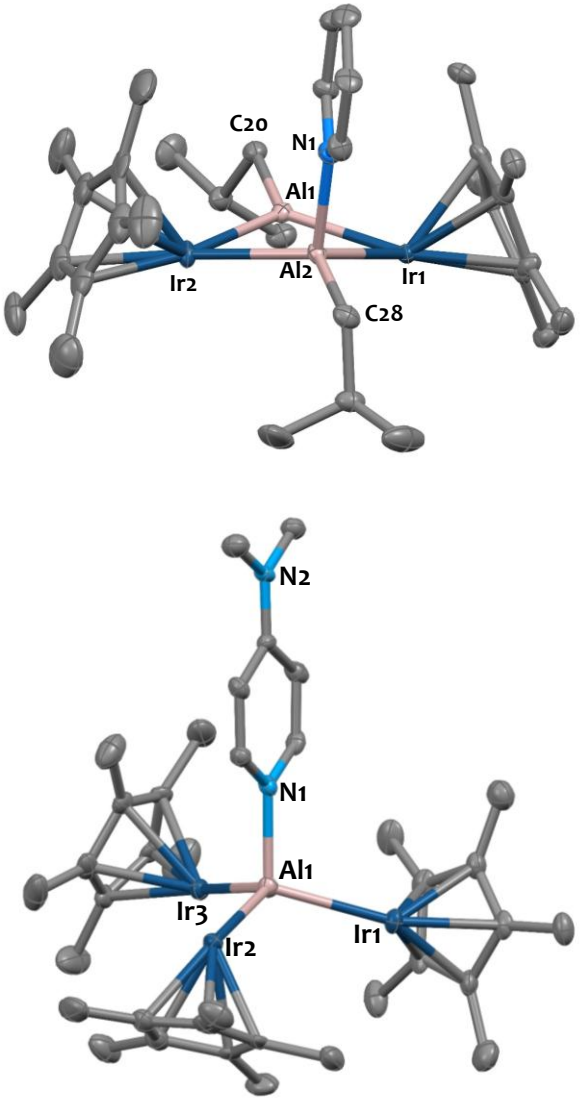


**Figure 6.** Solid-state molecular structures of compounds **5** (top) and **6** (bottom). Ellipsoids are represented with 30% probability. Hydrogen atoms have been omitted for clarity. Two independent molecules were found in the asymmetric units (Z'=2) of **5** and **6**, but one of them has been omitted for clarity. Selected bond distances (Å) and angles (°) have been averaged between both independent molecules in **5**: Ir1-Al1 2.426(3), Ir1-Al2 2.535(8), Ir2-Al1 2.422(8), Ir2-Al2 2.522(3), Al1-Al2 2.651(4), Al2-N1 2.070(3), Al1-C20 1.99(1), Al2-C28 1.99(1), (Ir1-Al1-Ir2-Al2)$_{centroid}$-Ir1-Cp*$_{centroid}$ 152.37, (Ir1-Al1-Ir2-Al2)$_{centroid}$-Ir2-Cp*$_{centroid}$ 154.58. In **6**: Ir-Al 2.56(2), Al-N 2.04(1), Ir-Al-Ir 114(3), Al-Ir-Cp*$_{centroid}$ 137(5).

The pyridine ligation to one Al Lewis acidic center is confirmed by the crystallographic structure of **5** (Figure 6-top). The Al2-N1 bond length (2.070(3) Å) is in the expected range.[60] The pyridine ligation to Al2 imparts a substantial distortion of the tetranuclear $Al_2Ir_2$ core with respect to **2**. This notably results in an elongation of the Ir-Al2 distances (2.53(1) Å) and a shortening of the Ir-Al1 distances (2.42(1) Å). This rearrangement could explain why a subsequent pyridine ligation onto Al1 is less favorable. Parameter α is equal to 153.48°, suggesting the presence of some terminal iridium-hydrides as discussed in the precedent cases. The coordination of pyridine onto **2** to form adduct **5** is in line with the presence of an accessible empty p-orbital on the aluminium centers.

On the opposite, no coordination of pyridine (even after heating to 80°C in $C_6D_6$ in presence of excess pyridine) was noticed onto complex **4**. We thus investigated the reaction of **4** with 4-dimethylaminopyridine (DMAP), which is more electron donating. This resulted in the coordination to the Al center to form adduct [{Cp*Ir(H)(μ-H$_2$)}$_3$Al(DMAP)], **6** (Scheme 4) isolated in 90% yield. The structure of **6** was notably confirmed by X-ray diffraction (Figure 6-bottom). The DMAP ligation to the Al site induces a pyramidalization of the Al center (average Ir-Al-Ir angle of 114(3)°; Al distance from the Ir$_3$ plane: 0.63(1) Å in **6** vs 0.04(4) Å in **4**) and results in an elongation of the Ir-Al distances (2.56(2) Å in **6** vs 2.47(1) in **4**), as expected. This indicates that the environment around the Al(III) center is flexible enough to accommodate an extra Lewis base donor, but that strong neutral donors cannot break such clusters to form ion pairs.

We then explored the reactivity of these Ir-Al clusters with Lewis acidic reagents. While reaction of compound **4** with stoichiometric amounts of *tris*(pentafluorophenyl)boron leads to a complex mixture of species that we were not able to isolate, treatment of **2** with B(C$_6$F$_5$)$_3$ in THF at 50°C for 2 days cleanly yields the de-alkylated compound **7** (Scheme 5). 1 equivalent of isobutene is evolved during the reaction (triplet at δ = 1.70 ppm and septuplet at δ = 4.62 ppm in THF-d$_8$),[85] as quantified by $^1$H-NMR reaction monitoring in THF-d$_8$ (Figure S26). B(C$_6$F$_5$)$_3$ is performing the abstraction of one hydride either directly from the isobutyl ligand or from complex **2**, inducing a beta-H elimination process releasing one equivalent of isobutene. The resulting cationic cluster **7** is associated with a HB(C$_6$F$_5$)$_3^-$ borate counter anion. This reaction confirms the high propensity of B(C$_6$F$_5$)$_3$ to perform hydride abstractions, as already described several times in the literature,[86,87] including by our group for alkyl aluminium species.[88] Note that the reaction was carried out in THF for solubility reasons since compound **7** is an ion pair, but also since THF can stabilize this dealkylated compound through coordination to the Lewis-acidic Al sites.

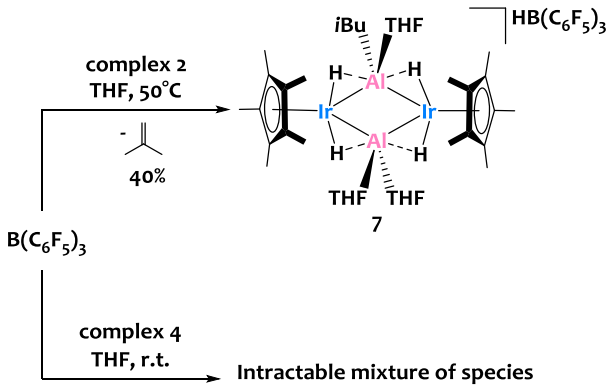


**Scheme 5. Reactivity of the Al-Ir heterobimetallic complexes 2 and 4 towards $B(C_6F_5)_3$.**

The identity of **7** was underpinned by multi-nuclei ($^1$H, $^{11}$B, $^{13}$C) solution NMR spectroscopy, infrared spectroscopy, elemental analysis and X-ray diffraction investigations. The $^1$H-NMR spectrum of **7** in THF-$d_8$ indicates the retaining of one isobutyl-aluminium fragment in the structure, as expected, since CH-*i*Bu (1.93 ppm), $CH_3$-*i*Bu (1.03 ppm) and $CH_2$-*i*Bu (0.51 ppm) signals are integrating for 1H, 6H, and 2H respectively. The $^{11}$B-NMR spectrum displays a typical doublet at $\delta$ = -23.60 ppm ($^1J_{B\text{-}H}$ = 94 Hz) matching with the $HB(C_6F_5)_3^-$ anion signature.[88–90] The DRIFT spectrum of **7** exhibits a typical H-B stretching band at 2364.1 cm$^{-1}$ which further confirms the formation of $HB(C_6F_5)_3^-$.[89] The solid-state molecular structure of **7** (Figure 7), determined by single-crystal XRD, shows that the two $\{Cp^*IrH_2\}^{2-}$ motifs are bridged by an $\{Al(iBu)(THF)\}^{2+}$ fragment on one side and an $\{Al(THF)_2\}^{3+}$ unit on the other side. The coordination geometries around the Al centers are pseudo tetrahedral with angles in the range [88.1-122.7°]. The $Al_2Ir_2$ core is almost planar (mean deviation from plane = 0.037(3) Å) and the Cp* ligands almost perpendicular to the metallic core plane ($\alpha$=176.28°), suggesting bridging hydrides. This geometry is comparable to that observed in **1**, in which the Al sites also adopt a pseudo-Td geometry. The Ir-Al2 distances (2.522(7) Å) are much longer than the Ir-Al1 distances (2.422(3) Å), as a result of an increased charge density on the de-alkylated Al1 site. These Ir-Al distances in **7** are much shorter than those in the fully-alkylated complex **1** (2.72(1) Å on average), which attest to a greater charge density on the Al sites, and stronger electronic donation from the $[Cp^*IrH_2]^{2-}$ fragments in **7**, as expected.

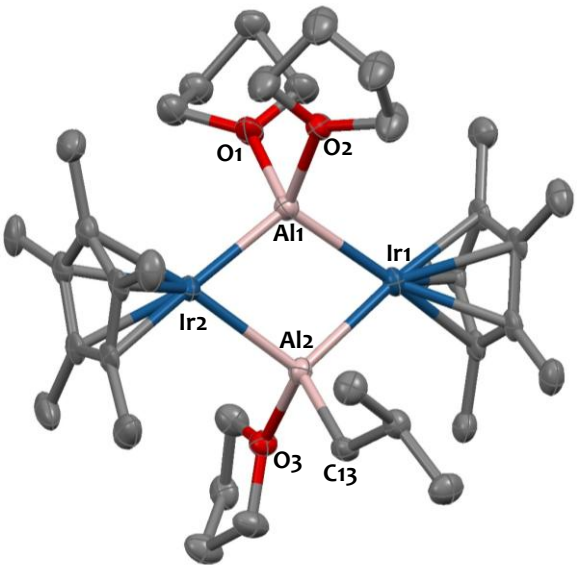


**Figure 7.** Solid-state molecular structure of **7**. Ellipsoids are represented with 30% probability. Hydrogen atoms and the $HB(C_6F_5)_3^-$ anion have been omitted for clarity. Selected bond distances (Å) and angles (°) Ir1-Al1 2.431(3), Ir1-Al2 2.521(2), Ir2-Al1 2.414(3), Ir2-Al2 2.524(2), Al1-O1 1.914(7), Al1-O2 1.950(7), Al2-O3 1.976(6), Al2-C13 1.983(8), Ir1-Al2-Ir2 105.21(9), Al1-Ir1-Al2 71.37(8), $(Ir1\text{-}Al1\text{-}Ir2\text{-}Al2)_{centroid}$-Ir1-$Cp^*_{centroid}$ 177.30, $(Ir1\text{-}Al1\text{-}Ir2\text{-}Al2)_{centroid}$-Ir2-$Cp^*_{centroid}$ 175.27.

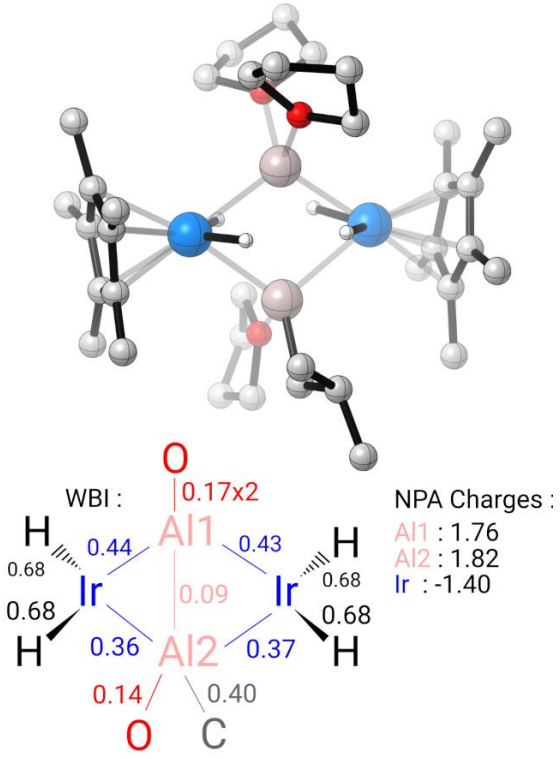


**Figure 8.** Most stable computed structure, NPA charges and Wiberg bond indexes of complex **7**.

For complex **7**, a conformational analysis has revealed four possible conformers in an energy range of 6.5 kcal.mol$^{-1}$ (see Figure S59). As for complex **2**, the most stable structure exhibits two hydrides in terminal position on each Ir center. The conformers with two terminal hydrides as well as two bridging hydrides Ir-H-Al or with four bridging hydrides Ir-H-Al are 3.0, 5.9 and 6.5 kcal.mol$^{-1}$ less stable, respectively. As experimentally observed, the calculated $Al_2Ir_2$ core is almost planar and the Ir-Al2 distances (2.533 and 2.597 Å) are much longer than the Ir-Al1 distances (2.453 and 2.460 Å). Compared to complex **1**, a larger negative charge is observed on Ir atoms (-1.405 vs. -0.958). The NPA charge on Al2 (+1.821) is also larger than in complex **1** (+1.776) while that on Al1 is similar in both complexes (+1.758).

Bergman and Rheingold have shown that, in the presence of strong bases (typically organolithium reagents), Ir-H species could be deprotonated, to yield highly reactive iridate derivatives.[76,77,79,80] Likewise, the reaction of $Cp^*IrH_4$ with benzyl potassium (Scheme 6 - bottom) quantitatively yields the potassium iridate species $\{K[Cp^*IrH_3]\}_n$, **8**, together with toluene. The structure of **8** was inferred from spectroscopic data which are similar to that of the lithium analogue, and especially a strongly shifted $^1$H NMR hydride signal at -19.29 ppm, versus -19.27 ppm in $[Cp^*IrH_3Li(pmdeta)]$,[91] and a shielded $^{13}C\{^1H\}$ NMR Cp* signal at 85.2 ppm, versus 87.4 ppm in $[Cp^*IrH_3Li(THF)_x]$.[92] The DRIFT spectrum of **8** displays a very intense and broad ν Ir-H band at σ = 2018 cm$^{-1}$ very close to that of $[Cp^*IrH_3Li(THF)_x]$ (σ = 2019 cm$^{-1}$).[92] Unfortunately, single crystals of **8** could not be obtained despite numerous attempts.

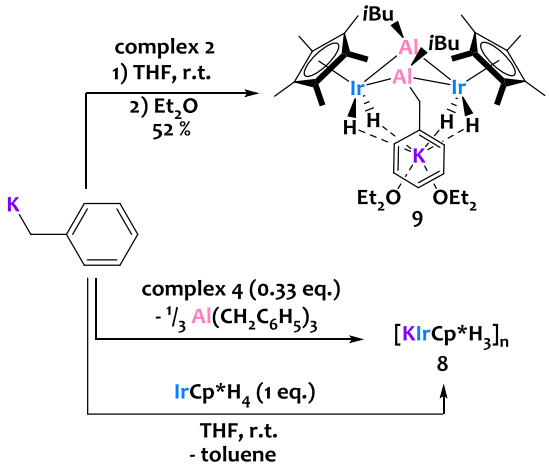


**Scheme 6. Reactivity of the Al-Ir heterobimetallic species 2 and 4 towards benzyl potassium.**

We then explored the reactivity of **2** and **4** towards benzyl potassium, yet in both cases we did not observe deprotonation of the hydrides. Instead, stoichiometric treatment of **2** with K-benzyl in THF leads to the nucleophilic addition of the benzyl anion onto the electrophilic aluminium center, to form the alkylated aluminate species **9** (Scheme 6). Complex **9** is isolated as yellow block crystals after a cold (-40°C) recrystallization in diethyl ether. The $^1$H-NMR spectrum of **9**, recorded in THF-$d_8$, displays two new aromatic signals at δ = 7.00 and 6.65 ppm, integrating for 4H and 1H respectively, confirming the coordination of the benzyl anion. The solid-state molecular structure of **9** (Figure 9), determined by X-ray diffraction, confirms the ligation of the benzyl fragment onto the Al center. The Al-$C_{benzyl}$ distance of 2.055(9) Å falls in the expected range.[93] The potassium cation is coordinated to the benzyl ring and stabilized by two diethyl ether molecules. This results in a noticeable distortion of the $[Ir\text{-}Al]_2$ core when compared to **2**, with an elongation of the Ir-Al2 distances and a shortening of the Ir-Al1 distances, alike what seen in the pyridine adduct **5**. The twisting of the Cp* rings (α = 154.0(1)°) is close to that in complex **2** (α = 151.5(1)°), and accordingly we propose terminal iridium hydrides.

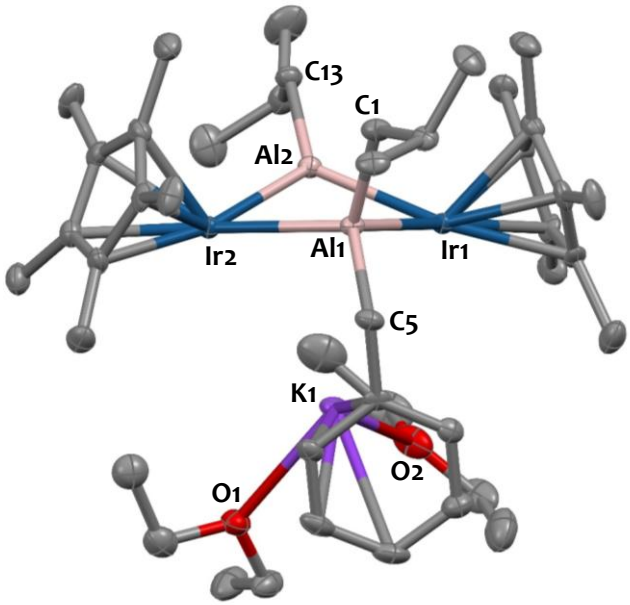


**Figure 9.** Solid-state molecular structure of **9**. Ellipsoids are represented with 30% probability. Hydrogen atoms have been omitted for clarity. Selected bond distances (Å) and angles (°) Ir1-Al1 2.650(2), Ir1-Al2 2.424(2), Ir2-Al1 2.601(2), Ir2-Al2 2.410(2), K1-O1 2.750(7), K1-O2 2.759(8), Al1-Al2 2.657(3), Al1-C1 2.017(9), Al1-C5 2.055(9), Al2-C13 1.977(9), Al2-Ir1-Al1 62.98(8), Ir2-Al1-Ir1 102.60(8) Al2-Ir2-Al1 63.93(8), (Ir1-Al1-Ir2-Al2)$_{centroid}$-Ir1-Cp*$_{centroid}$ 155.57, (Ir1-Al1-Ir2-Al2)$_{centroid}$-Ir2-Cp*$_{centroid}$ 152.34.

Treatment of cluster **4** with 3 equivalents of benzyl potassium neither leads to hydride deprotonation, nor nucleophilic addition. Instead, the transmetallated product $\{K[Cp^*IrH_3]\}_n$, **8**, is obtained together with $Al(CH_2C_6H_5)_3$. When **4** is treated with 1 or 2 equivalents of benzyl potassium, $\{K[Cp^*IrH_3]\}_n$, **8**, is also formed, together with a complex mixture of species, most likely due to benzyl transfer to aluminium and ligand redistribution. This reactivity is reminiscent of the $[Cp^*IrH_3]^-$/alkyl exchange process described above in the preparation of compound **3** from treatment of **4** with Al(*i*Bu)$_3$. Overall, these reactions show that the Al sites in these compounds are electrophilic

and act as benzyl anion acceptors, but also that further deprotonation of the hydrides in these iridate derivatives is not facile.

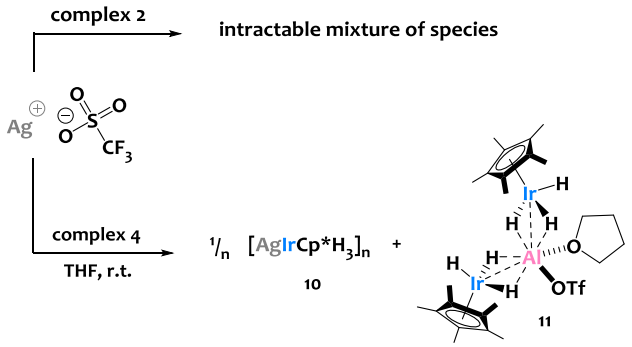


**Scheme 7. Reactivity of the Al-Ir heterobimetallic species 2 and 4 towards silver triflate.**

Finally, the reactivity of complex **4** towards silver(I) triflate was scrutinized. The addition of 1 equivalent of AgOTf onto **4**, in THF at room temperature, triggers the precipitation of a white solid, isolated in 93% yield by filtration, and corresponding to cluster $[AgCp^*IrH_3]_n$, noted **10** (Scheme 7). The DRIFT spectrum of **10** depicts an intense and broad metal-hydride stretching band shifted at lower wavenumbers when compared to compound **4** ($\sigma$ = 1917 $cm^{-1}$ in **10** *vs* $\sigma$ = 2015 & 2158 $cm^{-1}$ in **4**). This suggests the presence of bridging Ir–(μ-H)–Ag vibrators, in accord with literature data.[94] $^1H$ NMR studies, conducted in dried deuterated pyridine (for solubility reasons), unveil a hydride signal at $\delta_{1H}$ = -14.76 ppm slightly shifted towards downfield values compared to complex **4** ($\delta_{Ir\text{-}H}$ = -16.39 ppm in $C_6D_6$) and integrating for 3H (relative to Cp* signal). The solid-state structure of **10**, shown on Figure 10-bottom, reveals an unprecedented infinite 2D-network which can be seen as two parallel zigzag chains, alternating $[Ag]^+$ and $[Cp^*IrH_3]^-$ motifs, facing each other in a head-to-tail fashion (Figure 10-top), and fused together through argentophilic interactions.[95] Therein, the Ag1-Ag1# distance of 2.973(3) Å falls in the range of metallophilic $4d^{10}$-$4d^{10}$ interactions,[95] and thus compound **10** can be seen as $[Ag_2]^{2+}$ dications[94] stabilized by iridate fragments. This leads to 6-membered $Ag_4Ir_2$ metallacycles which are fused together to give the 2D-network represented schematically in Figure 10-top. The Ir1-Ag1-Ir1# angle is close to linearity (161.72(6)°), in agreement with the strong preference for linear coordination of Ag(I), while the Ag1-Ir1-Ag1# angle is 102.24(2)°. The Ir1-Ag1 distance of 2.7200(4) Å is longer than the sum of the respective metallic radii (Ag: 1.339 Å; Ir: 1.260 Å; sum = 2.599 Å).[64] In other crystallographically characterized silver iridium complexes featuring bridging hydrides, distances between Ir and Ag vary between 2.71 Å and 3.03 Å.[94,96–99] The Ir-Ag distance in **10** is in the low-end of this range, suggesting a strong interaction which is compatible with the presence of bridging hydrides. Complexes featuring unsupported bonds between Ir centers and $d^{10}$ Ag metal atoms are also known, and the Ir-Ag distances vary from 2.63 Å to 2.79 Å;[100–106] thus a direct metal-metal interaction in **10** cannot be totally excluded.

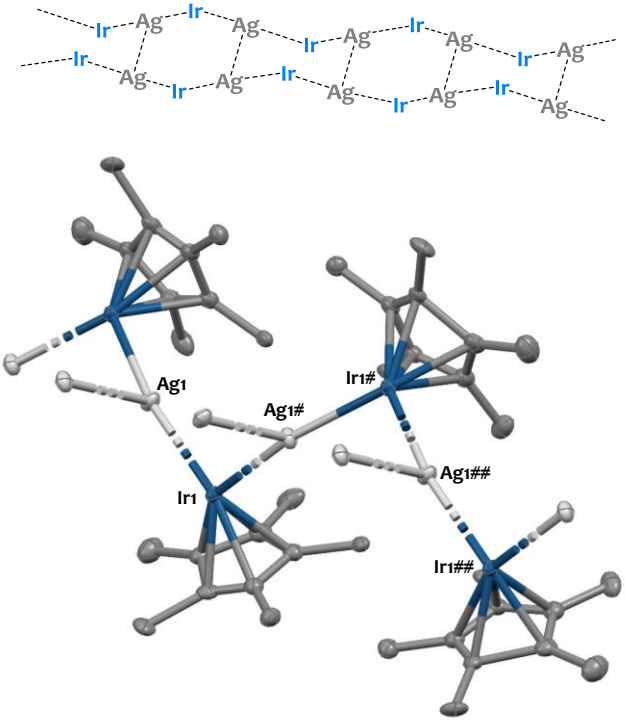


**Figure 10.** Top: schematic representation of the 2D fused metallacyclic network in **10**. Bottom: solid-state molecular structure of **10**. Ellipsoids are represented with 30% probability. Hydrogen atoms have been omitted for clarity. Selected bond distances (Å) and angles (°): Ir1-Ag1 2.7200(4), Ag1-Ag1# 2.973(3), Ag1-Ir1-Ag1# 102.24(2), Ir1-Ag1-Ir1# 161.72(6), Ir1-Ag1-Ag1# 99.14(3).

The reaction co-product, $[(IrCp^*H_3)_2Al(OTf)(THF)]$ **11** (Scheme 7) remains soluble in THF solution, and was isolated as an orange powder by removing volatiles from the reaction filtrate. The $^1H$ NMR spectrum of **11** displays new hydride and Cp* signals at $\delta$ = -17.41 ppm and $\delta$ = +2.12 ppm integrating respectively for 6H and 30H, in agreement with the proposed structure. In addition, the $^{19}F$ NMR spectrum of **11** depicts an upfield resonance at $\delta$ = -80.7 ppm, which supports the presence of a triflate moiety.[107,108] This is corroborated by the DRIFT spectrum of **11** which shows the presence of a S=O vibrator at $\sigma$ = 1347 $cm^{-1}$ and a C-F vibration band at $\sigma$ = 1201 $cm^{-1}$, which are typical of a triflate signature.[107] To unequivocally identify the 3D molecular structure of **11**, we performed a single-crystal X-ray diffraction study on the isolated crystalline material (obtained from cold recrystallization in $Et_2O$). The solid-state structure of **11** is represented on Figure 11. The $Al^{3+}$ center is surrounded by two $[Cp^*IrH_3]^-$ units and its coordination sphere is completed by the coordination two oxygen atoms: one from a monodentate triflate anion and the other from a THF molecule. The Ir-Al distances – averaged at 2.451(2) Å – are slightly longer than those in complex **3** (2.43(1) Å) and slightly shorter than those in complex **4** (2.48(1) Å). The noticeable Cp* rings twisting –

averaged at 136.8(1)° – is alike that found in **3** and **4** and suggests also the presence of hydrides in terminal position.

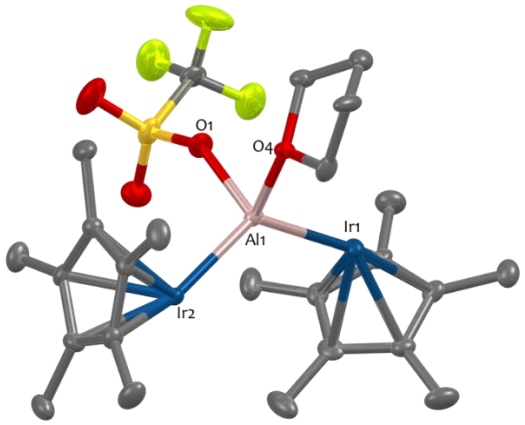


**Figure 11.** Solid-state molecular structure of **11**. Ellipsoids are represented with 30% probability. Hydrogen atoms have been omitted for clarity. Selected bond distances (Å) and angles (°): Ir1-Al1 2.449(3), Ir2-Al1 2.453(3), Al1-O1 1.895(6), Al1-O4 1.931(6), Ir1-Al1-Ir2 126.42(10), O1-Al1-Ir2 107.8(2), O4-Al1-Ir1 106.5(2), O1-Al1-O4 86.1(3), Al1-Ir1-Cp*$_{centroid}$ 136.80, Al1-Ir2-Cp*$_{centroid}$ 136.74.

In summary, the stoichiometric reaction of silver triflate with cluster **4** leads to the transmetallation of a $[Cp^*IrH_3]^-$ moiety from Al to Ag, and the coordination sphere of the aluminium center is substituted by a triflate ligand. Although silver salts are well-known oxidizing agents, no redox process occurs in this reaction. This reactivity provides evidence that the $[Cp^*IrH_3]^-$ anion is electron-donating and labile, with a higher affinity for the soft $Ag^+$ cation rather than the hard $Al^{3+}$ cation. The interaction of silver(I) with iridium hydride species forming unusual polynuclear silver-iridium derivatives were reported in a few occurences.[94,96–99,102] Given the importance of silver species in salt metathesis reactions, compound **10** could potentially serve as a synthetically useful source of $[Cp^*IrH_3]^-$ anions.

We also explored treatment of **2** with one equivalent of AgOTf, yet this leads to the formation of multiple products that we were unable to isolate. We did not detect Ag(0) in this reaction, which suggests the absence of redox processes. Rather, transmetallation / ligand redistribution phenomena, akin to that observed with **4**, are most likely at place.

## EXPERIMENTAL SECTION

### General Considerations.

Unless otherwise noted, all reactions were performed either using standard Schlenk line techniques or in an MBraun glovebox under an atmosphere of purified argon (<1 ppm $O_2$/$H_2O$). Glassware and cannulæ were stored in an oven at ~100 °C for at least 12 h prior to use. Toluene, *n*-pentane, octane, THF, and diethyl ether were purified by passage through a column of activated alumina, dried over Na/benzophenone, vacuum-transferred to a storage flask and freeze-pump-thaw degassed prior to use. Deuterated solvents were dried over Na/benzophenone (for THf-$d_8$, toluene-$d_8$ and $C_6D_6$) or refluxed over calcium hydride (for pyridine-$d_5$), then vacuum-transferred to a storage flask and freeze-pump-thaw degassed prior to use. Compounds $Cp^*IrH_4$,[92] were prepared according to the literature procedures. All other reagents were acquired from commercial sources and used as received.

### Characterization methods.

IR spectroscopy. Solid samples were prepared in a glovebox (diluted in dry KBr), sealed under argon in a DRIFT cell equipped with KBr windows and analyzed on a Nicolet 670 FT-IR spectrometer.

Elemental analyses were performed under inert atmosphere at Mikroanalytisches Labor Pascher, Germany.

X-ray structural determinations. Experimental details regarding XRD measurements are provided in SI. CCDC 2108876-2108884 and 2124619 contain the supplementary crystallographic data for this paper. These data are provided free of charge by the Cambridge Crystallographic Data Centre.

Computational methods. Experimental details regarding DFT studies are provided in SI.

NMR Spectroscopy. Solution NMR spectra were recorded on Bruker AV-300, AVQ-400 and AV-500 spectrometers. $^1H$ and $^{13}C$ chemical shifts were measured relative to residual solvent peaks, which were assigned relative to an external TMS standard set at 0.00 ppm. $^{11}B$ and $^{19}F$ chemical shifts are reported relative to $BF_3.OEt_2$ set at 0.00 ppm. $^1H$ and $^{13}C$ NMR assignments were confirmed by $^1H$–$^1H$ COSY and $^1H$–$^{13}C$ HSQC and HMBC experiment.

### Synthetic procedures.

Isolation of intermediate $[Cp^*IrH_3Al(^iBu)_2]_2$ **1**.

A 8 mL colorless pentane solution of $IrCp^*H_4$ (199.0 mg, 0.60 mmol, 1.0 eq.) was added dropwise to a 6 mL colorless pentane solution of triisobutylaluminium (152 µL, 119.0 mg, 0.60 mmol, 1.0 eq.). Within minutes, the solution turned yellowish. The solution was stirred for 2 hours at room temperature. Then, the volatiles were removed under vacuum, yielding *ca.* 250 mg of a crude yellow powder containing a mixture of species. This solid was dissolved in the minimum amount of pentane (*ca.* 2 mL), filtered, and stored at -40°C for 3 days yielding 50 mg of block-shaped yellow crystals of **1** suitable for XRD analysis. $^1H$ NMR (300 MHz, $C_6D_6$, 293 K) δ 2.21 (m, 4H, $CH_{iBu}$), 1.94 (s, 30H, $CH_{3Cp^*}$), 1.27 (d, 24H, $CH_{3\text{-}iBu}$), 0.55 (d, 8H, $CH_{2\text{-}iBu}$), -16.54 (s, 6H, Ir-H). Elemental analysis could not be performed on this unstable compound.

Synthesis of $[Cp^*IrH_2Al(iBu)]_2$ **2**.

A 20 mL colorless pentane solution of $IrCp^*H_4$ (979.0 mg, 2.95 mmol, 1.0 eq.) was added dropwise to a 30 mL colorless pentane solution of triisobutylaluminium (585.0 mg, 2.95 mmol, 1.0 eq.). Within minutes, the solution turned yellowish. The solution was stirred at room temperature

for 2 days. Then, the volatiles were removed under vacuum, yielding a yellow powder. The solid was dissolved in the minimum amount of pentane (*ca.* 6 mL), filtered, and stored at -40°C for 1 day yielding plate-shaped yellow crystals of **2** that were recovered by filtration and dried under vacuum (1.02 g, 83% yield). $^{1}$H NMR (500 MHz, $C_6D_6$, 293 K) δ 2.45 (m, 2H, $CH_{i\text{Bu}}$), 2.07 (s, 30H, $CH_{3\text{Cp*}}$), 1.35 (d, $^{3}J_{HH}$ = 6.6 Hz, 12H, $CH_{3\text{-}i\text{Bu}}$), 1.01 (d, $^{3}J_{HH}$ = 7.2 Hz, 4H, $CH_{2\text{-}i\text{Bu}}$), -16.68 (s, 4H, H-Ir). $^{13}$C{$^{1}$H} NMR (125 MHz, $C_6D_6$, 293 K) δ 93.54 ($C_{\text{Cp*}}$), 28.17.($CH_{3\text{-}i\text{Bu}}$), 27.70 ($CH_{2\text{-}i\text{Bu}}$), 27.00 ($CH_{i\text{Bu}}$), 11.47 ($CH_{3\text{-Cp*}}$). DRIFTS (293 K, cm$^{-1}$) σ 2977 (s), 2942 (s, *ν*C-H), 2910 (s, *ν*C-H), 2855 (s, *ν*C-H), 1990 (s, *ν*Ir-H), 1455 (s). Elemental analysis calcd (%) for $C_{28}H_{52}Al_2Ir_2$: C 40.66, H 6.34. Found: C 40.79, H 6.36.

Synthesis of [(Cp*IrH$_3$)$_2$Al(*i*Bu)] **3**.

*From triisobutylaluminium.* A 6 mL pentane solution of IrCp*H$_4$ (501.2 mg, 1.51 mmol, 2.0 eq.) was added dropwise (within 10 minutes) into a 4 mL colorless pentane solution of triisobutylaluminium (150.3 mg, 0.76 mmol, 1.0 eq.). The resulting light yellowish solution was stirred at room temperature for 17 hours. This procedure triggered precipitation of an off-yellow solid that was removed by filtration (*ca.* 130 mg). The filtrate was collected and the volatiles were removed *in vacuo*, yielding 390 mg of **3** as a pale yellow powder (69 % yield). Yellow needle single crystals of **3** suitable for XRD analysis were grown by slow evaporation of a cold (T= -40°C) and saturated pentane solution of **3**.

*From compound **2**.* A 0.4 mL $C_6D_6$ solution of IrCp*H$_4$ (11.8 mg, 35.6 µmol, 2.0 eq.) was added into a 0.3 mL $C_6D_6$ solution of complex **2** (14.5 mg, 17.5 µmol, 1.0 eq.). The resulting yellow solution was sealed under argon in a 2.5 mL J-Young NMR tube and kept at room temperature for 24 hours. NMR analysis of the crude reaction shows a complete consumption of **2** with evolution of isobutane along with the formation of product **3**. $^{1}$H NMR (400 MHz, $C_6D_6$, 293 K) δ 2.49 (m, 1H, $CH_{i\text{Bu}}$), 2.03 (s, 30H, $CH_{3\text{Cp*}}$), 1.29 (d, $^{3}J_{HH}$ = 6.4 Hz, 6H, $CH_{3\text{-}i\text{Bu}}$), 0.56 (d, $^{3}J_{HH}$ = 7.0 Hz, 2H, $CH_{2\text{-}i\text{Bu}}$), -16.64 (s, 6H, H-Ir). $^{13}$C{$^{1}$H} NMR (125 MHz, $C_6D_6$, 293 K) δ 93.88 ($C_{\text{Cp*}}$), 42.51 ($CH_{2\text{-}i\text{Bu}}$), 28.24 ($CH_{3\text{-}i\text{Bu}}$), 27.56 ($CH_{i\text{Bu}}$), 11.28 ($CH_{3\text{-Cp*}}$). DRIFTS (293 K, cm$^{-1}$) σ 2977 (s), 2955 (s, *ν*C-H), 2910 (s, *ν*C-H), 2857 (s, *ν*C-H), 2151 (s, *ν*Ir-H), 2014 (s, *ν*Ir-H), 1456 (s), 1386 (s), 1033 (s). Elemental analysis calcd (%) for $C_{28}H_{52}Al_2Ir_2$: C 38.69, H 6.09. Found: C 38.63, H 6.12.

Synthesis of [(Cp*IrH$_3$)$_3$Al] **4**.

*From triisobutylaluminium.* A 7 mL light yellow toluene solution of IrCp*H$_4$ (502.6 mg, 1.52 mmol, 3.0 eq.) was added dropwise into a 4 mL colorless pentane solution of triisobutylaluminium (99.1 mg, 0.50 mmol, 1.0 eq.). The resulting light-yellow solution was sealed in a 80 mL Schlenck vessel and stirred at 50°C for 1 week yielding a bright orange solution. The volatiles were removed *in vacuo*, yielding a brownish solid. This powder was dissolved in the minimum amount of pentane (*ca.* 6 mL), filtered, and stored at T=-40°C for 1 day yielding **4** as colorless block crystals (269.5 mg, 53% yield). The resulting filtrate was concentrated and stored at T=-40°C for 2 weeks yielding a second crop of **4** as crystals (80.0 mg, 16% yield; combined yield = 69%).

*From compound **3**.* A 7 mL pentane/toluene (5/2) solution of IrCp*H$_4$ (176 mg, 0.53 mmol, 1.2 eq.) was added dropwise into a 4 mL yellow pentane suspension of complex **3** (346 mg, 0.46 mmol, 1.0 eq.). The resulting solution was stirred at T=65°C for 2 days producing a deep orange-brown solution. Volatiles were removed under vacuum, yielding a brownish powder which was dissolved in the minimum of pentane (*ca.* 5.5 mL), filtered, and stored at T=-40°C for 18 hours, yielding **4** as colorless crystals (320 mg, 68% yield). $^{1}$H NMR (500 MHz, $C_6D_6$, 293 K) δ 2.11 (s, 45H, $CH_{3\text{Cp*}}$), -16.38 (s, 9H, H-Ir). $^{13}$C{$^{1}$H} NMR (125 MHz, $C_6D_6$, 293 K) δ 93.62 ($C_{\text{Cp*}}$), 11.26 ($CH_{3\text{-Cp*}}$). DRIFTS (293 K, cm$^{-1}$) σ 2980 (s, *ν*C-H), 2957 (s, *ν*C-H), 2912 (s, *ν*C-H), 2158 (s, *ν*Ir-H), 2015 (s, *ν*Ir-H), 1476 (m), 1456 (m), 1385 (m). Elemental analysis calcd (%) for $C_{45}H_{54}AlIr_3$: C 35.38, H 5.34. Found: C 35.45, H 5.36.

Synthesis of [IrCp*H$_2$(Py)Al(*i*Bu)]$_2$ **5**.

A 0.5 mL colorless pentane solution of pyridine (12.6 µL, 0.17 mmol, 1.1 eq.) was added dropwise into a 7 mL yellow pentane solution of **2** (130.0 mg, 0.16 mmol, 1.0 eq.). In the course of the addition, the solution turned to a blood red mixture that was further stirred at room temperature for 20 minutes. The volatiles were removed under vacuum, yielding 130 mg of a red solid. This powder was dissolved in the minimum amount of toluene (*ca.* 1.0 mL), filtered, and stored at -40°C for 18 hours, yielding **5** as dark orange needle crystals (60 mg, 42% isolated yield). $^{1}$H NMR (500 MHz, $C_6D_6$, 293 K) δ 8.72 (d, 2H, $CH_{ortho\text{-}Py}$), 6.81 (t, 1H, $CH_{para\text{-}Py}$), 6.55 (t, 2H, $CH_{meta\text{-}Py}$), 2.55 (m, 2H, $CH_{i\text{Bu}}$), 1.92 (s, 30H, $CH_{3\text{Cp*}}$), 1.47 (d, $^{3}J_{HH}$ = 6.4 Hz, 12H, $CH_{3\text{-}i\text{Bu}}$) , 0.93 (d, $^{3}J_{HH}$ =6.7 Hz, 4H, $CH_{2\text{-}i\text{Bu}}$), -16.89 (s, 4H, H-Ir). $^{13}$C{$^{1}$H} NMR (125 MHz, $C_6D_6$, 293 K) δ 148.27 ($CH_{ortho\text{-Py}}$), 137.69 ($CH_{para\text{-Py}}$), 124.02 ($CH_{meta\text{-Py}}$), 92.16 ($C_{\text{Cp*}}$), 28.68 ($CH_{3\text{-}i\text{Bu}}$), 27.91 ($CH_{2\text{-}i\text{Bu}}$), 27.15 ($CH_{i\text{Bu}}$), 11.12 ($CH_{3\text{-Cp*}}$). DRIFTS (293 K, cm$^{-1}$) σ 2942 (s, *ν*C-H), 2910 (s, *ν*C-H), 2856 (s, *ν*C-H), 2110 (m, *ν*Ir-H), 2005 (m, *ν*Ir-H), 1607 (m), 1484 (m), 1439 (m), 1377 (m), 1158 (m). Elemental analysis calcd (%) for $C_{33}H_{57}Al_2Ir_2N$: C 43.74, H 6.34, N 1.55. Found: C 43.16, H 6.34, N 1.52.

Synthesis of [{Cp*Ir(H)(µ-H$_2$)}$_3$Al(DMAP)], **6**.

A 1 mL colorless toluene solution of 4-dimethylaminopyridine (11.9 mg, 0.097 mmol, 1.0 eq.) was added dropwise into a 2 mL colorless pentane solution of compound **4** (100.3 mg, 0.098 mmol, 1.0 eq.). The resulting solution was stirred at room temperature for 1 hour. Then, volatiles were removed under vacuum yielding a white solid (c.a. 110 mg). The solid was dissolved in a mixture of pentane/toluene (15/1 mL), filtered, ant stired at T=-40°C, yielding colorless block-shaped crystals of **6** (100.0 mg, 90% yield). $^{1}$H NMR (500 MHz, $C_6D_6$, 293 K) δ 8.64 (d, $^{3}J_{H\text{-}H}$ = 5.0 Hz, 2H, $CH_{ortho\text{-DMAP}}$), 6.05 (d, $^{3}J_{H\text{-}H}$ = 5.0 Hz, 2H, $CH_{meta\text{-DMAP}}$), 2.15 (s, 6H, $CH_3$-N), 2.14 (s, 45H, $CH_{3\text{-Cp*}}$), -

16.47 (s, 9H, H-Ir). $^{13}C\{^1H\}$ NMR (125 MHz, $C_6D_6$, 293 K) δ 150.52 ($CH_{ortho\text{-}DMAP}$), 106.28 ($CH_{meta\text{-}DMAP}$), 93.25 ($C_{Cp^*}$), 38.28 ($CH_3$-N), 11.20 ($CH_{3\text{-}Cp^*}$). DRIFTS (293 K, $cm^{-1}$) σ 3080 (m, $\nu_{C\text{-}H}$), 2957 (s, $\nu_{C\text{-}H}$), 2907 (s, $\nu_{C\text{-}H}$), 2149 (s, $\nu_{Ir\text{-}H}$), 2111 (s, $\nu_{Ir\text{-}H}$), 1626 (m), 1538 (m), 1448 (m), 1383 (m), 1232 (s).

Synthesis of complex **7**.

A 4 mL colorless THF solution of $B(C_6F_5)_3$ (93.4 mg, 0.18 mmol, 1.0 eq.) was added dropwise to a 6 mL yellow THF solution of **2** (150.2 mg, 0.18 mmol, 1.0 eq.). The resulting yellow solution was stirred at room temperature for 19 hours. The reaction mixture was then heated at 50°C for 5 hours. Then, the volatiles were removed under vacuum, yielding a light-yellow powder. This solid was dissolved in 2 mL of pentane, 250 µL of THF was added to the solution which was filtered and stored at -40°C for 14 hours. This procedure yielded compound **7** as plate-shaped yellow crystals (110 mg, 40% yield). $^1H$ NMR (500 MHz, THF-$d_8$, 293 K) δ 3.62 (t, 8H, $CH_{2\text{-}THF}$), 2.03 (s, 30H, $CH_{3Cp^*}$), 1.93 (m, 1H, $CH_{i\text{Bu}}$), 1.77 (m, 8H, $CH_{2\text{-}THF}$), 1.04 (d, $^3J_{HH}$ = 6.6 Hz, 6H, $CH_{3\text{-}i\text{Bu}}$) , 0.51 (d, $^3J_{HH}$ = 6.6 Hz, 2H, $CH_{2\text{-}i\text{Bu}}$), -16.92 (s, 4H, H-Ir). $^{13}C\{^1H\}$ NMR (125 MHz, THF-$d_8$, 293 K) δ 93.00, ($C_{Cp^*}$), 68.03 ($C_{THF}$), 28.08 ($CH_{2\text{-}i\text{Bu}}$), 27.13 ($CH_{3\text{-}i\text{Bu}}$), 26.18 ($CH_{i\text{Bu}}$), 25.61 ($C_{THF}$), 11.33 ($CH_{3\text{-}Cp^*}$).$^{11}B$-NMR (160 MHz, THF-$d_8$, RT) δ -23.60 (d, $^1J_{BH}$ = 94 Hz). DRIFTS (293 K, $cm^{-1}$) σ 2956 (s, *ν*C-H), 2918 (s, *ν*C-H), 2852 (s, *ν*C-H), 2364 (m, *ν*B-H), 2137 (m, *ν*Ir-H), 1640 (m), 1509 (s), 1462 (s). Elemental analysis calcd (%) for $C_{57}H_{73}Al_2BF_{15}Ir_2O_3$: C 44.45, H 4.78. Found: C 44.31, H 4.89.

Reaction of complex **2** with $B(C_6F_5)_3$ monitored by quantitative NMR spectroscopy

A 0.5 mL colorless THF-$d_8$ colorless solution of $B(C_6F_5)_3$ (13.2 mg, 25.8 µmol, 1.0 eq.) and durene (12.2 mg, 90.9 µmol, 3.5 eq.) – used as internal standard – was added into a 2.0 mL yellow THF-$d_8$ solution of **2** (21.3 mg, 25.8 µmol, 1.0 eq.). The resulting solution was sealed under argon in a 2.5 mL J-Young NMR tube. Then, the tube was kept at room temperature for 3 days and heated at 50°C for 5 hours. Regularly, the tube was analysed by $^1H$-NMR and $^{19}F$-NMR spectroscopy. This leads to the disappearance of the $^1H$ NMR signals from **2** and the appearance of $^1H$ NMR signals corresponding to complex **3** and isobutene. At completion, the amount of **3** (21.4 µmol, 0.83 eq.) and released isobutene (24.6 µmol, 0.95 eq.) were determined by signal integration respective to the durene internal standard (see Figure S26).

Formation of [IrCp*$H_3$K], complex **8**

From IrCp*$H_4$. A 0.4 mL red THF-$d_8$ solution of K-benzyl (3.6 mg, 27.6 µmol, 1.0 eq.) was added dropwise into a 0.4 mL colorless THF-$d_8$ solution of IrCp*$H_4$ (10.0 mg, 30.2 µmol, 1.1 eq.). The resulting yellowish solution was sealed in a J-Young NMR tube and left at room temperature for 6 hours. Analysis of the solution revealed the quantitative formation of product **8** along with toluene. $^1H$ NMR (500 MHz, THF$d_8$, 293 K) δ 2.13 (s, 15H, $CH_{3Cp^*}$), -19.29 (s, 3H, H-Ir). $^{13}C\{^1H\}$ NMR (125 MHz, THF-$d_8$, 293 K) δ 85.17 ($C_{Cp^*}$), 12.54 ($CH_{3\text{-}Cp^*}$). DRIFTS (293 K, $cm^{-1}$) σ 2973 (s, *ν*C-H), 2949 (s, *ν*C-H), 2898 (s, *ν*C-H), 2850 (s, *ν*C-H), 2072 (s, *ν*Ir-H), 2018 (s, *ν*Ir-H), 1474 (m), 1378 (m), 1234 (m), 1027 (m).

From **4**. A 3.5 mL red THF solution of benzyl potassium (76.7 mg, 0.589 mmol, 3.0 eq.) was added dropwise into a 3.5 mL colorless THF solution of complex **4** (200.6 mg, 0.197 mmol, 1 eq.). The resulting yellowish solution was stirred at room temperature for 24 hours. THF volatiles were removed under vacuum yielding a yellow solid (250 mg). This solid was analyzed by NMR spectroscopy (recorded in THF-$d_8$) and revealed the formation of **8** along with $Al(CH_2C_6H_5)_3$.

Synthesis of complex **9**.

A 4 mL red THF solution of benzyl potassium (27.8 mg, 0.21 mmol, 1.0 eq.) was added dropwise to a 6 mL yellow THF solution of **2** (175.5 mg, 0.21 mmol, 1.0 eq.). The resulting yellow solution was stirred for 18 hours at room temperature. Then, the volatiles were removed under vacuum, yielding a yellow powder. This solid was dissolved in the minimum of diethyl ether (*ca.* 2 mL), filtered and stored at 40°C for 3 hours yielding **9** as yellow block crystals (120 mg, 52% yield). $^1H$ NMR (500 MHz, THF-$d_8$, 293 K) δ 7.00 (d, 4H, $CH_{Ar}$), 6.65 (m, 1H, $CH_{Ar}$), 3.39 (q, $^3J_{HH}$ = 6.9 Hz, $CH_{2\text{-}Et2O}$), 2.13 (s, 2H, $CH_{2\text{-}benzyl}$), 2.11 (s, 30H, $CH_{3Cp^*}$), 2.04 (m, 2H, $CH_{i\text{Bu}}$), 1.12 (t, $^3J_{HH}$ = 7.0 Hz $CH_{3\text{-}Et2O}$), 0.98 (d, $^3J_{HH}$ = 6.4 Hz, 12H, $CH_{3\text{-}i\text{Bu}}$), 0.57 (d, 4H, $CH_{2\text{-}i\text{Bu}}$), -18.35 (s, 4H, H-Ir). $^{13}C\{^1H\}$ NMR (125 MHz, THF-$d_8$, 293 K) δ 156.00 ($C_{Ar}$), 127.71 ($CH_{Ar}$), 127.13 ($CH_{Ar}$), 117.77 ($CH_{Ar}$), 91.65, ($C_{Cp^*}$), 66.14 ($CH_{2\text{-}Et2O}$), 28.83 ($CH_{i\text{Bu}}$), 28.17 ($CH_{2\text{-}i\text{Bu}}$), 26.67 ($CH_{3\text{-}i\text{Bu}}$), 25.62 ($CH_{2\text{-}benzene}$), 15.50 ($CH_{3\text{-}Et2O}$), 11.77 ($CH_{3\text{-}Cp^*}$). DRIFTS (293 K, $cm^{-1}$) σ 3062 (w, *ν*C-H), 2971 (s, *ν*C-H), 2941 (s, *ν*C-H), 2913 (s, *ν*C-H), 2848 (s, *ν*C-H), 2140 (m, *ν*Ir-H), 2001 (m, *ν*Ir-H), 1965 (m, *ν*Ir-H), 1593 (m), 1483 (m), 1453 (m), 1379 (m), 1105 (m). Elemental analysis calcd (%) for $C_{43}H_{79}Al_2Ir_2KO_2$: C 46.71, H 7.20. Found: C 46.27, H 7.08.

Synthesis of complexes **10** and **11**.

A 1.5 mL colorless THF solution of silver triflate (50.2 mg, 0.195 mmol, 1.0 eq.) was added dropwise into a 1.5 mL yellow THF solution of compound **4** (200.4 mg, 0.197 mmol, 1.0 eq.). In the course of the addition, the solution turned deep-orange and some off-white solids precipitated. The resulting mixture was stirred at room temperature for one hour leading to the precipitation of further white materials that were recovered using a P4 sintered glass filter funnel, washed with 1.5 mL of THF, and dried in *vacuo* for 2 hours. The resulting microcrystalline white powder corresponds to compound **10** (82 mg, 93 %). The volatiles from the orange filtrate were removed under vacuum yielding product **11** as an orange powder (159 mg, 90% yield). Plate-shaped single crystals of **11** suitable for XRD studies were grown from a cold (T=-40°C) and saturated diethyl ether solution of **11**. Characterization data for

complex **10**. $^{1}$H NMR (400 MHz, pyridine-$d_5$, 293 K) δ 2.31 (s, 60H, $CH_{3Cp^*}$),-14.76 (s, 12H, H-Ir). $^{13}C\{^{1}H\}$ NMR (100 MHz, pyridine-$d_5$, 293 K) δ 91.55 ($C_{Cp^*}$), 13.01 ($CH_{3\text{-}Cp^*}$). DRIFTS (293 K, $cm^{-1}$) σ 2980 (s, *ν*C-H), 2945 (s, *ν*C-H), 2895 (s, *ν*C-H), 1917 (s, *ν*Ir-H), 1467 (m), 1375 (m), 866 (s). Elemental analysis calcd (%) for $C_{10}H_{18}AgIr$: C 27.40, H 4.14, Ir 43.8. Found: C 27.49, H 4.15, Ir 42.7. Characterization data for complex **11**. $^{1}$H NMR (400 MHz, THF-$d_8$, 293 K) δ 2.12 (s, 30H, $CH_{3Cp^*}$), -17.41 (s, 6H, H-Ir). $^{19}$F NMR (282 MHz, THF-$d_8$, 293 K) δ -80.65 (s). $^{13}C\{^{1}H\}$ NMR (100 MHz, THF-$d_8$, 293 K) δ 94.92 ($C_{Cp^*}$), 11.05 ($CH_{3\text{-}Cp^*}$). DRIFTS (293 K, $cm^{-1}$) σ 2986 (s, *ν*C-H), 2962 (s, *ν*C-H), 2914 (s, *ν*C-H), 2152 (s, *ν*Ir-H), 2070 (s, *ν*Ir-H), 1347 (s, *ν*S=O), 1238 (m), 1201 (s, *νC*-F), 1032 (m). Elemental analysis calcd (%) for $C_{25}H_{44}AlIr_2F_3O_4S$: C 33.03, H 4.88. Found: C 32.92, H 4.81.

## CONCLUSIONS

This study has proven the utility of the stepwise alkane elimination strategy for the preparation of a family of well-defined iridium aluminium polyhydrides of various nuclearities and compositions, which were fully characterized. The hydrides in $Cp^*IrH_4$ are acidic and are inducing the protonolysis of aluminium isobutyl moieties. The obtained tri- and tetranuclear Ir/Al complexes have original structures, which are best described as iridate units held together by cationic Al(III) moieties. For instance, complex **4** is a rare example of an Al site surrounded by only 6 hydrogens, yet contrary to most transition metal aluminohydride complexes which can be considered as $[AlH_{x+3}]^{x-}$ and $LnM^{+}$ moieties, the situation here is reversed and **4** is best described as an ate-complex formed of $[Cp^*IrH_3]^-$ fragments surrounding an $Al^{3+}$ cation.[109–111] This is corroborated by reactivity studies, which have proven that the hydrides are always retained at the iridium sites and that the $[Cp^*IrH_3]^-$ moieties are labile and could be transmetallated to yield potassium or silver derivatives of potential synthetic interest.

DFT calculations have shown that the bonding situation can vary in these systems, from 3-centre 2-electron hydride-bridged Lewis adducts of the form Ir–H→Al, to direct polarized metal–metal interaction from donation of *d*-electrons of Ir to the Al metal (Z-type ligand), and both types of interactions are most probably at place to some extent in each of these complexes.[109]

The subsequent deprotonation of the $[Cp^*IrH_3]^-$ fragments in this series of complexes is more difficult, and was only observed in the formation of complex **2**. The resulting $[Cp^*IrH_2]^{2-}$ units in **2** are highly basic, and are protonated back in the presence of $Cp^*IrH_4$, which is more favourable than the Al-*i*Bu protonolysis in that case. The aluminium sites in these derivatives are electrophilic and can interact with Lewis bases or anionic ligands such as alkyls, as in the formation of **5, 6** or **8**. Such alkyl transfer at aluminium appears key in the ligand redistribution phenomena, as is exemplified by the reaction of complex **3** with $Al(iBu)_3$ leading to **1**, again attesting to the lability of these polymetallic assemblies. These metal/ligand redistribution phenomena pave the way towards the preparation of more diverse architectures through metal substitution.

## ASSOCIATED CONTENT

**Supporting Information**. NMR and IR spectroscopy, X-ray crystallography and computational data. This material is available free of charge via the Internet at http://pubs.acs.org.

## AUTHOR INFORMATION

### Corresponding Author

* clement.camp@univ-lyon1.fr

### Author Contributions

All authors have given approval to the final version of the manuscript.

## ACKNOWLEDGMENT

We thank Laurent Veyre and Nesrine Oueslati for their help with the spectroscopic analyses. We gratefully acknowledge financial support from the CNRS-MOMENTUM 2017 program. CalMip is acknowledged for a generous grant of computing time (CALMIP-EOS grant 0833). L.M. is a member of the Institut Universitaire de France.

## REFERENCES

(1) Dhayal, R. S.; Van Zyl, W. E.; Liu, C. W. Copper Hydride Clusters in Energy Storage and Conversion. *Dalton Trans.* **2019**, *48* (11), 3531–3538. https://doi.org/10.1039/c8dt04639e.

(2) Ma, L.; Zhou, T.; Li, J.; Chen, H. Aluminum-Silicon Hydride Clusters for Prospective Hydrogen Storage. *Int. J. Hydrogen Energy* **2019**, *44* (48), 26459–26468. https://doi.org/10.1016/j.ijhydene.2019.08.109.

(3) Sclüth, F.; Bogdanović, B.; Felderhoff, M. Light Metal Hydrides and Complex Hydrides for Hydrogen Storage. *Chemical Communications*. The Royal Society of Chemistry October 15, 2004, pp 2249–2258. https://doi.org/10.1039/b406522k.

(4) Schlapbach, L.; Züttel, A. Hydrogen-Storage Materials for Mobile Applications. *Nature*. Nature Publishing Group November 15, 2001, pp 353–358. https://doi.org/10.1038/35104634.

(5) Shima, T.; Luo, G.; Hu, S.; Luo, Y.; Hou, Z. Experimental and Computational Studies of Dinitrogen Activation and Hydrogenation at a Tetranuclear Titanium Imide/Hydride Framework. *J. Am. Chem. Soc.* **2019**, *141* (6), 2713–2720. https://doi.org/10.1021/jacs.8b13341.

(6) Shima, T.; Yang, J.; Luo, G.; Luo, Y.; Hou, Z. Dinitrogen Activation and Hydrogenation by C5Me4SiMe3-Ligated Di- And Trinuclear Chromium Hydride Complexes. *J. Am. Chem. Soc.* **2020**, *142* (19), 9007–9016. https://doi.org/10.1021/jacs.0c02939.

(7) Shima, T.; Hu, S.; Luo, G.; Kang, X.; Luo, Y.; Hou, Z. Dinitrogen Cleavage and Hydrogenation by a Trinuclear Titanium Polyhydride Complex. *Science (80-. ).* **2013**, *340* (6140), 1549–1552. https://doi.org/10.1126/science.1238663.

(8) Guru, M. M.; Shima, T.; Hou, Z. Conversion of Dinitrogen to Nitriles at a Multinuclear Titanium Framework. *Angew. Chemie - Int. Ed.* **2016**, *55* (40), 12316–12320. https://doi.org/10.1002/anie.201607426.

(9) Nakamae, K.; Tanaka, M.; Kure, B.; Nakajima, T.; Ura, Y.; Tanase, T. A Fluxional Cu8H6 Cluster Supported by Bis(Diphenylphosphino)Methane and Its Facile Reaction with CO2. *Chem. - A Eur. J.* **2017**, *23* (40), 9457–9461. https://doi.org/10.1002/chem.201702071.

(10) Tang, Q.; Lee, Y.; Li, D. Y.; Choi, W.; Liu, C. W.; Lee, D.; Jiang, D.

E. Lattice-Hydride Mechanism in Electrocatalytic CO2 Reduction by Structurally Precise Copper-Hydride Nanoclusters. *J. Am. Chem. Soc.* **2017**, *139* (28), 9728–9736. https://doi.org/10.1021/jacs.7b05591.

(11) Nguyen, T. A. D.; Goldsmith, B. R.; Zaman, H. T.; Wu, G.; Peters, B.; Hayton, T. W. Synthesis and Characterization of a Cu14 Hydride Cluster Supported by Neutral Donor Ligands. *Chem. - A Eur. J.* **2015**, *21* (14), 5341–5344. https://doi.org/10.1002/chem.201500422.

(12) Gieshoff, T. N.; Chakraborty, U.; Villa, M.; Jacobi von Wangelin, A. Alkene Hydrogenations by Soluble Iron Nanocluster Catalysts. *Angew. Chemie - Int. Ed.* **2017**, *56* (13), 3585–3589. https://doi.org/10.1002/anie.201612548.

(13) Ohki, Y.; Shimizu, Y.; Araake, R.; Tada, M.; Sameera, W. M. C.; Ito, J.-I.; Nishiyama, H. Co 6 H 8 (P i Pr 3 ) 6 : A Cobalt Octahedron with Face-Capping Hydrides. *Angew. Chemie - Int. Ed.* **2016**, *128* (51), 16053–16057. https://doi.org/10.1002/ange.201608262.

(14) Sun, C.; Mammen, N.; Kaappa, S.; Yuan, P.; Deng, G.; Zhao, C.; Yan, J.; Malola, S.; Honkala, K.; Häkkinen, H.; et al. Atomically Precise, Thiolated Copper-Hydride Nanoclusters as Single-Site Hydrogenation Catalysts for Ketones in Mild Conditions. *ACS Nano* **2019**, *13* (5), 5975–5986. https://doi.org/10.1021/acsnano.9b02052.

(15) Shima, T.; Luo, Y.; Stewart, T.; Bau, R.; McIntyre, G. J.; Mason, S. A.; Hou, Z. Molecular Heterometallic Hydride Clusters Composed of Rare-Earth and d-Transition Metals. *Nat. Chem.* **2011**, *3* (10), 814–820. https://doi.org/10.1038/nchem.1147.

(16) Shima, T.; Hou, Z. Rare Earth/d-Transition Metal Heteromultimetallic Polyhydride Complexes Based on Half-Sandwich Rare Earth Moieties. *Organometallics* **2009**, *28* (7), 2244–2252. https://doi.org/10.1021/om900024q.

(17) Garçon, M.; Bakewell, C.; Sackman, G. A.; White, A. J. P.; Cooper, R. I.; Edwards, A. J.; Crimmin, M. R. A Hexagonal Planar Transition-Metal Complex. *Nature* **2019**, *574* (7778), 390–393. https://doi.org/10.1038/s41586-019-1616-2.

(18) Shima, T.; Sugimura, Y.; Suzuki, H. Heterometallic Trinuclear Polyhydrido Complexes Containing Ruthenium and a Group 9 Metal, [Cp *3Ru2M(M3-H)(μ-H) 3] (M = Ir or Rh; Cp* = H5-C 5Me5): Synthesis, Structure, and Site Selectivity in Reactions with Phosphines. *Organometallics* **2009**, *28* (3), 871–881. https://doi.org/10.1021/om8010432.

(19) Cadenbach, T.; Bollermann, T.; Gemel, C.; Fischer, R. A. Synthesis and Structure of Electron Rich Ruthenium Polyhydride Complexes and Clusters Containing AlCp* and GaCp*. *Dalton Trans.* **2009**, No. 2, 322–329. https://doi.org/10.1039/b807917j.

(20) Rhodes, L. F.; Bansemer, R. L.; Folting, K.; Huffman, J. C.; Caulton, K. G. A Heterometallic Cluster with Extreme Hydride Content: H24Cu6Re4(PPh3)82+. *Inorganica Chim. Acta* **1992**, *191* (1), 31–34. https://doi.org/10.1016/S0020-1693(00)80323-0.

(21) Sizov, A. I.; Zvukova, T. M.; Belsky, V. K.; Bulychev, B. M. Aluminium Zirconium (+3 and +4) Heterometallic Hydrido Complexes of Compositions [(H5-C5H5)2Zr(μ-H)] 2(μ-H)AlCl2 and [(H5-C5H5)2ZrH(μ-H) 2]3Al. *J. Organomet. Chem.* **2001**, *619* (1–2), 36–42. https://doi.org/10.1016/S0022-328X(00)00564-7.

(22) Ohashi, M.; Matsubara, K.; Iizuka, T.; Suzuki, H. Trinuclear Ruthenium Polyhydride Complexes with a Triply Bridging Ligand: [{(H5-C5Me5)Ru}3- (M3-M)(μ-H)3(M3-H)] (M = Li, MgiPr, and ZnEt) and [{(H5-C5Me5)Ru}3 (M3-M)(μ-H)3] (M = AlEt and GaMe). *Angew. Chemie - Int. Ed.* **2003**, *42* (8), 937–940. https://doi.org/10.1002/anie.200390249.

(23) Martin, D.; Beckerle, K.; Schnitzler, S.; Spaniol, T. P.; Maron, L.; Okuda, J. Discrete Magnesium Hydride Aggregates: A Cationic Mg13H18 Cluster Stabilized by NNNN-Type Macrocycles. *Angew. Chemie - Int. Ed.* **2015**, *54* (13), 4115–4118. https://doi.org/10.1002/anie.201411612.

(24) Sun, C.; Teo, B. K.; Deng, C.; Lin, J.; Luo, G. G.; Tung, C. H.; Sun, D. Hydrido-Coinage-Metal Clusters: Rational Design, Synthetic Protocols and Structural Characteristics. *Coord. Chem. Rev.* **2021**, *427*, 213576. https://doi.org/10.1016/j.ccr.2020.213576.

(25) Lee, S.; Bootharaju, M. S.; Deng, G.; Malola, S.; Häkkinen, H.; Zheng, N.; Hyeon, T. [Pt 2 Cu 34 (PET) 22 Cl 4 ] 2– : An Atomically Precise, 10-Electron PtCu Bimetal Nanocluster with a Direct Pt–Pt Bond . *J. Am. Chem. Soc.* **2021**, *143* (31), 12100–12107. https://doi.org/10.1021/jacs.1c04002.

(26) Yang, J.; Pang, R.; Song, D.; Li, M. B. Tailoring Silver Nanoclusters: Via Doping: Advances and Opportunities. *Nanoscale Adv.* **2021**, *3* (9), 2411–2422. https://doi.org/10.1039/d1na00077b.

(27) Akanuma, Y.; Imaoka, T.; Sato, H.; Yamamoto, K. Silver in the Center Enhances Room-Temperature Phosphorescence of a Platinum Sub-Nanocluster by 18 Times. *Angew. Chemie - Int. Ed.* **2021**, *60* (9), 4551–4554. https://doi.org/10.1002/anie.202012921.

(28) Du, X.; Jin, R. Atomic-Precision Engineering of Metal Nanoclusters. *Dalton Trans.* **2020**, *49* (31), 10701–10707. https://doi.org/10.1039/d0dt01853h.

(29) Bootharaju, M. S.; Chang, H.; Deng, G.; Malola, S.; Baek, W.; Häkkinen, H.; Zheng, N.; Hyeon, T. Cd12Ag32(SePh)36: Non-Noble Metal Doped Silver Nanoclusters. *J. Am. Chem. Soc.* **2019**, *141* (21), 8422–8425. https://doi.org/10.1021/jacs.9b03257.

(30) Ghosh, A.; Mohammed, O. F.; Bakr, O. M. Atomic-Level Doping of Metal Clusters. *Acc. Chem. Res.* **2018**, *51* (12), 3094–3103. https://doi.org/10.1021/acs.accounts.8b00412.

(31) Cesari, C.; Berti, B.; Bortoluzzi, M.; Femoni, C.; Iapalucci, M. C.; Zacchini, S. Heterometallic Ni-Pt Chini-Type Carbonyl Clusters: An Example of Molecular Random Alloy Clusters. *Inorg. Chem.* **2021**, *60* (12), 8811–8825. https://doi.org/10.1021/acs.inorgchem.1c00752.

(32) Cesari, C.; Shon, J.-H.; Zacchini, S.; Berben, L. A. Metal Carbonyl Clusters of Groups 8–10: Synthesis and Catalysis. *Chem. Soc. Rev.* **2021**. https://doi.org/10.1039/d1cs00161b.

(33) Ciabatti, I.; Femoni, C.; Iapalucci, M. C.; Longoni, G.; Zacchini, S. Bimetallic Nickel-Cobalt Hexacarbido Carbonyl Clusters [H 6-NNi 22Co 6C 6(CO) 36] n- (n = 3-6) Possessing Polyhydride Nature and Their Base-Induced Degradation to the Monoacetylide [Ni 9CoC 2(CO) 16- x] 3- (x = 0, 1). *Organometallics* **2012**, *31* (12), 4593–4600. https://doi.org/10.1021/om300412d.

(34) Riddlestone, I. M.; Rajabi, N. A.; Macgregor, S. A.; Mahon, M. F.; Whittlesey, M. K. Well-Defined Heterobimetallic Reactivity at Unsupported Ruthenium-Indium Bonds. *Chem. - A Eur. J.* **2018**, *24* (7), 1732–1738. https://doi.org/10.1002/chem.201705796.

(35) Riddlestone, I. M.; Rajabi, N. A.; Lowe, J. P.; Mahon, M. F.; Macgregor, S. A.; Whittlesey, M. K. Activation of H2 over the Ru-Zn Bond in the Transition Metal-Lewis Acid Heterobimetallic Species [Ru(IPr)2(CO)ZnEt]+. *J. Am. Chem. Soc.* **2016**, *138* (35), 11081–11084. https://doi.org/10.1021/jacs.6b05243.

(36) Espinal-Viguri, M.; Varela-Izquierdo, V.; Miloserdov, F. M.; Riddlestone, I. M.; Mahon, M. F.; Whittlesey, M. K. Heterobimetallic Ruthenium-Zinc Complexes with Bulky N-Heterocyclic Carbenes: Syntheses, Structures and Reactivity. *Dalton Trans.* **2019**, *48* (13), 4176–4189. https://doi.org/10.1039/c8dt05023f.

(37) Butovskii, M. V; Tok, O. L.; Wagner, F. R.; Kempe, R. Bismetallocenes: Lanthanoid-Transition-Metal Bonds through Alkane Elimination. *Angew. Chemie - Int. Ed.* **2008**, *47* (34), 6469–6472. https://doi.org/10.1002/anie.200800407.

(38) Butovskii, M. V; Tok, O. L.; Bezugly, V.; Wagner, F. R.; Kempe, R. Molecular Lanthanoid-Transition-Metal Cluster through C-H Bond Activation by Polar Metal-Metal Bonds. *Angew. Chemie - Int. Ed.* **2011**, *50* (33), 7695–7698. https://doi.org/10.1002/anie.201102363.

(39) Marsella, J. A.; Huffman, J. C.; Caulton, K. G.; Longato, B.; Norton, J. R. Dinuclear Elimination as a Route to Unusual Bridging Carbonyls and Acetyls in Heterobimetallic Complexes. *J. Am. Chem. Soc.* **1982**, *104* (23), 6360–6368. https://doi.org/10.1021/ja00387a034.

(40) Sobaczynski, A. P.; Obenauf, J.; Kempe, R. Alkane Elimination Reactions between Yttrium Alkyls and Tungsten Hydrides. *Eur. J. Inorg. Chem.* **2014**, *2014* (7), 1211–1217. https://doi.org/10.1002/ejic.201301476.

(41) Butovskii, M. V.; Döring, C.; Bezugly, V.; Wagner, F. R.; Grin, Y.; Kempe, R. Molecules Containing Rare-Earth Atoms Solely Bonded by Transition Metals. *Nat. Chem.* **2010**, *2* (9), 741–744. https://doi.org/10.1038/nchem.718.

(42) Lassalle, S.; Jabbour, R.; Schiltz, P.; Berruyer, P.; Todorova, T. K.; Veyre, L.; Gajan, D.; Lesage, A.; Thieuleux, C.; Camp, C. Metal–Metal Synergy in Well-Defined Surface Tantalum–Iridium Heterobimetallic Catalysts for H/D Exchange Reactions. *J. Am. Chem. Soc.* **2019**, *141* (49), 19321–19335. https://doi.org/10.1021/jacs.9b08311.

(43) Lassalle, S.; Jabbour, R.; Del Rosal, I.; Maron, L.; Fonda, E.; Veyre, L.; Gajan, D.; Lesage, A.; Thieuleux, C.; Camp, C. Stepwise Construction of Silica-Supported Tantalum/Iridium Heteropolymetallic Catalysts Using Surface Organometallic Chemistry. *J. Catal.* **2020**, *392*, 287–301. https://doi.org/10.1016/j.jcat.2020.10.016.

(44) Del Rosal, I.; Lassalle, S.; Dinoi, C.; Thieuleux, C.; Maron, L.; Camp, C. Mechanistic Investigations via DFT Support the Cooperative Heterobimetallic C-H and O-H Bond Activation across TaIr Multiple Bonds. *Dalton Trans.* **2021**, *50* (2), 504–510. https://doi.org/10.1039/d0dt03818k.

(45) Cowie, B. E.; Tsao, F. A.; Emslie, D. J. H. Synthesis and Platinum Complexes of an Alane-Appended 1,1′-Bis(Phosphino)Ferrocene Ligand. *Angew. Chemie Int. Ed.* **2015**, *54* (7), 2165–2169. https://doi.org/10.1002/anie.201410828.

(46) Rudd, P. A.; Liu, S.; Gagliardi, L.; Young, V. G.; Lu, C. C. Metal-Alane Adducts with Zero-Valent Nickel, Cobalt, and Iron. *J. Am. Chem. Soc.* **2011**, *133* (51), 20724–20727. https://doi.org/10.1021/ja2099744.

(47) Brewster, T. P.; Nguyen, T. H.; Li, Z.; Eckenhoff, W. T.; Schley, N. D.; DeYonker, N. J. Synthesis and Characterization of Heterobimetallic Iridium–Aluminum and Rhodium–Aluminum Complexes. *Inorg. Chem.* **2018**, *57* (3), 1148–1157. https://doi.org/10.1021/ACS.INORGCHEM.7B02601.

(48) Liu, H.-Y.; Schwamm, R. J.; Hill, M. S.; Mahon, M. F.; McMullin, C. L.; Rajabi, N. A. Ambiphilic Al–Cu Bonding. *Angew. Chemie Int. Ed.* **2021**, *60* (26), 14390–14393. https://doi.org/10.1002/ANIE.202104658.

(49) Devillard , M.; Nicolas, E.; Ehlers, A. W.; Backs, J.; Mallet-Ladeira, S.; Bouhadir , G.; Slootweg, J. C.; Uhl, W.; Bourissou , D. Dative Au→Al Interactions: Crystallographic Characterization and Computational Analysis. *Chem. - A Eur. J.* **2015**, *21* (1), 74–79. https://doi.org/10.1002/chem.201405610.

(50) Ekkert, O.; White, A. J. P.; Toms, H.; Crimmin, M. R. Addition of Aluminium, Zinc and Magnesium Hydrides to Rhodium(III). *Chem. Sci.* **2015**, *6* (10), 5617–5622. https://doi.org/10.1039/c5sc01309g.

(51) Hooper, T. N.; Lau, S.; Chen, W.; Brown, R. K.; Garçon, M.; Luong, K.; Barrow, N. S.; Tatton, A. S.; Sackman, G. A.; Richardson, C.; et al. The Partial Dehydrogenation of Aluminium Dihydrides. *Chem. Sci.* **2019**, *10* (35), 8083–8093. https://doi.org/10.1039/c9sc02750e.

(52) Lau, S.; White, A. J. P.; Casely, I. J.; Crimmin, M. R. Tunable Binding of Dinitrogen to a Series of Heterobimetallic Hydride Complexes. *Organometallics* **2018**, *37* (23), 4521–4526. https://doi.org/10.1021/acs.organomet.8b00340.

(53) Morisako, S.; Watanabe, S.; Ikemoto, S.; Muratsugu, S.; Tada, M.; Yamashita, M. Synthesis of A Pincer-IrV Complex with A Base-Free Alumanyl Ligand and Its Application toward the Dehydrogenation of Alkanes. *Angew. Chemie - Int. Ed.* **2019**, *58* (42), 15031–15035. https://doi.org/10.1002/anie.201909009.

(54) Hara, N.; Saito, T.; Semba, K.; Kuriakose, N.; Zheng, H.; Sakaki, S.; Nakao, Y. Rhodium Complexes Bearing PAlP Pincer Ligands. *J. Am. Chem. Soc.* **2018**, *140* (23), 7070–7073. https://doi.org/10.1021/jacs.8b04199.

(55) Mears, K. L.; Stennett, C. R.; Taskinen, E. K.; Knapp, C. E.; Carmalt, C. J.; Tuononen, H. M.; Power, P. P. Molecular Complexes Featuring Unsupported Dispersion-Enhanced Aluminum-Copper and Gallium-Copper Bonds. *J. Am. Chem. Soc.* **2020**, *142* (47), 19874–19878. https://doi.org/10.1021/jacs.0c10099.

(56) Bajo, S.; Alférez, M. G.; Alcaide, M. M.; López-Serrano, J.; Campos, J. Metal-Only Lewis Pairs of Rhodium with s, p and d-Block Metals. *Chem. - A Eur. J.* **2020**, *26* (70), 16833–16845. https://doi.org/10.1002/chem.202003167.

(57) Lai, Q.; Bhuvanesh, N.; Ozerov, O. V. Unexpected B/Al Transelementation within a Rh Pincer Complex. *J. Am. Chem. Soc.* **2020**, *142* (50), 20920–20923. https://doi.org/10.1021/jacs.0c09344.

(58) Nakamura, T.; Suzuki, K.; Yamashita, M. Aluminabenzene-Rh and -Ir Complexes: Synthesis, Structure, and Application toward Catalytic C-H Borylation. *J. Am. Chem. Soc.* **2017**, *139* (49), 17763–17766. https://doi.org/10.1021/jacs.7b11127.

(59) Hicks, J.; Mansikkamäki, A.; Vasko, P.; Goicoechea, J. M.; Aldridge, S. A Nucleophilic Gold Complex. *Nat. Chem.* **2019**, *11* (3), 237–241. https://doi.org/10.1038/s41557-018-0198-1.

(60) Escomel, L.; Del Rosal, I.; Maron, L.; Jeanneau, E.; Veyre, L.; Thieuleux, C.; Camp, C. Strongly Polarized Iridiumδ--Aluminumδ+Pairs: Unconventional Reactivity Patterns Including CO2Cooperative Reductive Cleavage. *J. Am. Chem. Soc.* **2021**, *143* (12), 4844–4856. https://doi.org/10.1021/jacs.1c01725.

(61) T. Golden, J.; H. Peterson, T.; L. Holland, P.; G. Bergman, R.; A. Andersen, R.; Golden, J. T.; Peterson, T. H.; Holland, P. L.; Bergman, R. G.; Andersen, R. A. Adduct Formation and Single and Double Deprotonation of Cp*(PMe3)Ir(H)2 with Main Group Metal Alkyls and Aryls: Synthesis and Structure of Three Novel Ir-Al and Ir-Mg Heterobimetallics. *J. Am. Chem. Soc.* **1998**, *120* (1), 223–224. https://doi.org/10.1021/ja973230v.

(62) Oishi, M.; Oshima, M.; Suzuki, H. A Study on Zr-Ir Multiple Bonding Active for C-H Bond Cleavage. *Inorg. Chem.* **2014**, *53* (13), 6634–6654. https://doi.org/10.1021/ic500258g.

(63) Cotton, F. A.; Murillo, C. A.; Walton, R. A. *Multiple Bonds between Metal Atoms*, 3rd ed.; Cotton, F. A., Murillo, C. A., Walton, R. A., Eds.; Springer Science and Business Media: New York, USA, 2005.

(64) Pauling, L. Atomic Radii and Interatomic Distances in Metals. *J. Am. Chem. Soc.* **1947**, *69* (3), 542–553. https://doi.org/10.1021/ja01195a024.

(65) Shima, T. Heterobimetallic Polyhydride Complex Containing Ruthenium and Iridium. Synthesis and Site-Selectivity in the Reaction with Unsaturated Hydrocarbons. *Organometallics* **2000**, *19* (13), 2420–2422. https://doi.org/10.1021/om000270q.

(66) Shima, T.; Ito, J. I.; Suzuki, H. Synthesis, Characterization, and Structure Determination of the Heterobimetallic Polyhydride Complexes (C5Me5)Ru(μ-H)3MH3(C 5Me5) (M = Mo, W) Containing Group VI and Group VIII Metals. *Organometallics* **2001**, *20* (1), 10–12. https://doi.org/10.1021/om000769k.

(67) Rozenel, S. S.; Padilla, R.; Camp, C.; Arnold, J. Unusual Activation of H2 by Reduced Cobalt Complexes Supported by a PNP Pincer Ligand. *Chem. Commun.* **2014**, *50* (20), 2612–2614.

(68) Dohmeier, C.; Robl, C.; Tacke, M.; Schnöckel, H. The Tetrameric Aluminum(I) Compound [{Al(H5-C5Me5)}4]. *Angew. Chemie - Int. Ed.* **1991**, *30* (5), 564–565. https://doi.org/10.1002/anie.199105641.

(69) Bag, P.; Weetman, C.; Inoue, S. Experimental Realisation of Elusive Multiple-Bonded Aluminium Compounds: A New Horizon in Aluminium Chemistry. *Angew. Chemie Int. Ed.* **2018**, *57* (44), 14394–14413. https://doi.org/10.1002/anie.201803900.

(70) Bag, P.; Porzelt, A.; Altmann, P. J.; Inoue, S. A Stable Neutral Compound with an Aluminum-Aluminum Double Bond. *J. Am. Chem. Soc.* **2017**, *139* (41), 14384–14387. https://doi.org/10.1021/jacs.7b08890.

(71) Pluta, C.; Pörschke, K.-R.; Krüger, C.; Hildenbrand, K. An Al□Al One-Electronπ Bond. *Angew. Chemie Int. Ed. English* **1993**, *32* (3), 388–390. https://doi.org/10.1002/anie.199303881.

(72) Wright, R. J.; Phillips, A. D.; Power, P. P. The [2 + 4] Diels-Alder Cycloadditon Product of a Probable Dialuminene, Ar′AlAlAr′ (Ar′ = C6H3- 2,6-Dipp 2; Dipp = C6H3-2,6-Pri2), with Toluene. *J. Am. Chem. Soc.* **2003**, *125* (36), 10784–10785. https://doi.org/10.1021/ja034478p.

(73) Agou, T.; Nagata, K.; Tokitoh, N. Synthesis of a Dialumene-Benzene Adduct and Its Reactivity as a Synthetic Equivalent of a Dialumene. *Angew. Chemie Int. Ed.* **2013**, *52* (41), 10818–10821. https://doi.org/10.1002/anie.201305228.

(74) Li, B.; Kundu, S.; Zhu, H.; Keil, H.; Herbst-Irmer, R.; Stalke, D.; Frenking, G.; Andrada, D. M.; Roesky, H. W. An Open Route to Asymmetric Substituted Al–Al Bonds Using Al(I)- and Al(III)-Precursors. *Chem. Commun.* **2017**, *53* (17), 2543–2546. https://doi.org/10.1039/C7CC00325K.

(75) Weetman, C.; Porzelt, A.; Bag, P.; Hanusch, F.; Inoue, S. Dialumenes – Aryl vs. Silyl Stabilisation for Small Molecule Activation and Catalysis. *Chem. Sci.* **2020**, *11* (18), 4817–4827. https://doi.org/10.1039/D0SC01561J.

(76) Gilbert, T. M.; Bergman, R. G. Synthesis of Trimethylphosphine-Substituted (Pentamethylcyclopentadienyl)Iridium Hydride Complexes; Protonation and Deprotonation of (C5(CH3)5)Ir(P(CH3)3)H2. *J. Am. Chem. Soc.* **1985**, *107* (12), 3502–3507. https://doi.org/10.1021/ja00298a017.

(77) Peterson, T. H. Deprotonation of the Transition Metal Hydride (H5-C5Me5)(PMe3)IrH2. Synthesis and Chemistry of the Strongly Basic Lithium Iridate (H5-C5Me5)(PMe3)Ir(H)(Li). *Organometallics* **1999**, *18* (10), 2005–2020. https://doi.org/10.1021/om980945d.

(78) Suárez, E.; Plou, P.; Gusev, D. G.; Martín, M.; Sola, E. Cationic, Neutral, and Anionic Hydrides of Iridium with PSiP Pincers. *Inorg. Chem.* **2017**, *56* (12), 7190–7199. https://doi.org/10.1021/acs.inorgchem.7b00833.

(79) Miranda-Soto, V.; Grotjahn, D. B.; DiPasquale, A. G.; Rheingold, A. L. Imidazol-2-Yl Complexes of Cp*Ir as Bifunctional Ambident Reactants. *J. Am. Chem. Soc.* **2008**, *130* (40), 13200–13201. https://doi.org/10.1021/ja804713u.

(80) Hughes, R. P.; Williamson, A.; Sommer, R. D.; Rheingold, A. L. The First Transition Metal Complex of Tetrafluorobenzyne: Ir(H5-C5Me5) (PMe3)(H2-C6F4) [11]. *Journal of the American Chemical Society*. American Chemical Society 2001, pp 7443–7444. https://doi.org/10.1021/ja010992o.

(81) Peterson, T. H.; Golden, J. T.; Bergman, R. G. Evidence for the Intervention of Different C-H Activating Intermediates in the Irradiation of (H5-C5Me5)(PMe3) IrH2 and the Reaction of (H5-C5Me5)(PMe3)Ir(H)(Cl) with Strong Base. *J. Am. Chem. Soc.* **2001**, *123* (3), 455–462. https://doi.org/10.1021/ja0024993.

(82) Etkin, N.; Stephan, D. W. The Zirconocene Dihydride-Alane Adducts [(Cp′)2ZrH(μ-H)2]3Al and [(Cp′)2ZrH(μ-H)2]2AlH (Cp′) Me3SiC5H4). *Organometallics* **1998**, *17* (4), 763–765. https://doi.org/10.1021/om970849x.

(83) Vajeeston, P.; Ravindran, P.; Kjekshus, A.; Fjellvåg, H. Tructural Stability and Electronic Structure for Li3AlH6. *Phys. Rev. B - Condens. Matter Mater. Phys.* **2004**, *69* (2), 1–4. https://doi.org/10.1103/PhysRevB.69.020104.

(84) Brinks, H. W.; Hauback, B. C. The Structure of Li3AlD6. *J. Alloys Compd.* **2003**, *354* (1–2), 143–147. https://doi.org/10.1016/S0925-8388(02)01348-8.

(85) Camp, C.; Kefalidis, C. E.; Pécaut, J.; Maron, L.; Mazzanti, M. Controlled Thermolysis of Uranium (Alkoxy)Siloxy Complexes: A Route to Polymetallic Complexes of Low-Valent Uranium. *Angew. Chemie - Int. Ed.* **2013**, *52* (48), 12646–12650. https://doi.org/10.1002/anie.201307291.

(86) Erker, G. Special Reactions. *Dalt. Trans.* **2005**, No. 11, 1883–1890.

(87) Dagorne, S.; Le Bideau, F.; Welter, R.; Bellemin-Laponnaz, S.; Maisse-François, A. Well-Defined Cationic Alkyl- And Alkoxide-Aluminum Complexes and Their Reactivity with $ε$-Caprolactone and Lactides. *Chem. - A Eur. J.* **2007**, *13* (11), 3202–3217. https://doi.org/10.1002/chem.200601112.

(88) Dardun, V.; Escomel, L.; Jeanneau, E.; Camp, C. On the Alcoholysis of Alkyl-Aluminum(III) Alkoxy-NHC Derivatives: Reactivity of the Al-Carbene Lewis Pair versus Al-Alkyl. *Dalton Trans.* **2018**, *47* (31), 10429–10433. https://doi.org/10.1039/c8dt01498a.

(89) Litters, S.; Kaifer, E.; Enders, M.; Himmel, H. J. A Boron-Boron Coupling Reaction between Two Ethyl Cation Analogues. *Nat. Chem.* **2013**, *5* (12), 1029–1034. https://doi.org/10.1038/nchem.1776.

(90) Ullrich, M.; Lough, A. J.; Stephan, D. W. Reversible, Metal-Free, Heterolytic Activation of H2 at Room Temperature. *J. Am. Chem. Soc.* **2009**, *131* (1), 52–53. https://doi.org/10.1021/ja808506t.

(91) Gilbert, T. M.; Bergman, R. G. NMR Spectra of (C5(CH3)5)IrH2SiMe3Li(Pmdeta) and (C5(CH3)5)IrH3Li(Pmdeta): The First Direct Observation of Resolved 7Li-1H Coupling. *J. Am. Chem. Soc.* **1985**, *107* (22), 6391–6393. https://doi.org/10.1021/ja00308a040.

(92) Gilbert, T. M.; Hollander, F. J.; Bergman, R. G. (Pentamethylcyclopentadienyl)Iridium Polyhydride Complexes: Synthesis of Intermediates in the Mechanism of Formation of (C5(CH3)5)IrH4 and the Preparation of Several Iridium(V) Compounds. *J. Am. Chem. Soc.* **1985**, *107* (12), 3508–3516. https://doi.org/10.1021/ja00298a018.

(93) Kurumada, S.; Takamori, S.; Yamashita, M. An Alkyl-Substituted Aluminium Anion with Strong Basicity and Nucleophilicity. *Nat. Chem.* **2020**, *12* (1), 36–39. https://doi.org/10.1038/s41557-019-0365-z.

(94) Gorol, M.; Mösch-Zanetti, N. C.; Roesky, H. W.; Noltemeyer, M.; Schmidt, H. G. Unprecedented Stabilisation of the AG22+-Ion by Two Hydrido-Iridium(III) Complexes. *Chem. Commun.* **2003**, No. 1, 46–47. https://doi.org/10.1039/b209884a.

(95) Schmidbaur, H.; Schier, A. Argentophilic Interactions. *Angew. Chemie Int. Ed.* **2015**, *54* (3), 746–784. https://doi.org/10.1002/ANIE.201405936.

(96) Braunstein, P.; Carneiro, T. M. G.; Matt, D.; Tiripicchio, A.; Camellini, M. T. Synthesis and Structure of [(Ph3P)3Ir(M3-H)(μ-H)2Ag2(OSO2CF3)(H2O)]-(CF3SO3), a Complex with a Bent Ag-Ir-Ag Chain. *Angew. Chemie Int. Ed. English* **1986**, *25* (8), 748–749. https://doi.org/10.1002/ANIE.198607481.

(97) Bachechi, F. X-Ray Structural Analysis of the Polyhydride Complex Salt [(Ph3P)3Ir(μ-H)3Ag(μ-H)3Ir(Ph3P)3][O3SCF3]. *J. Organomet. Chem.* **1994**, *474* (1–2), 191–197. https://doi.org/10.1016/0022-328X(94)84065-2.

(98) Albinati, A.; Anklin, C.; Janser, P.; Lehner, H.; Matt, D.; Pregosin, P. S.; Venanzi, L. M. Gold and Silver Hydrides: Synthesis of Heterobimetallic Ir-m (m = Au, Ag) Complexes and X-Ray Crystal Structures of [(PPH3)Au(μ-H)IrH2(PPH3)3](BF4) and [(PPH3)Ag(μ-h)IrH2(PPH3)3](CF3s03). *Inorg. Chem.* **1989**, *28* (6), 1105–1111. https://doi.org/10.1021/ic00305a021.

(99) Maekawa, M.; Kubo, Y.; Sugimoto, K.; Okubo, T.; Kuroda-Sowa, T.; Munakata, M. Heterometallic AgI-IrIII Hydride Coordination Polymers Bridged by IrIII Metalloligands. *Eur. J. Inorg. Chem.* **2016**, *2016* (1), 78–91.

https://doi.org/10.1002/ejic.201500996.

(100) Kimura, T.; Ishiwata, K.; Kuwata, S.; Ikariya, T. Trapping of a Doubly Unsaturated Dinuclear Iridium(II) Sulfonylimido Complex with Phosphine and Lewis Acidic Group 11 and 12 Metals. *Organometallics* **2012**, *31* (3), 1204–1207. https://doi.org/10.1021/OM201218J.

(101) Sykes, A.; Mann, K. R. Thermal Encapsulation and Photochemical Deencapsulation of Ag(I) by [Ir2(Dimen)4](PF6)2 (Dimen = 1,8-Diisocyanomenthane). X-Ray Crystal Structure of [AgIr2(Dimen)4](PF6)3.2DMSO. *J. Am. Chem. Soc.* **1988**, *110* (24), 8252–8253. https://doi.org/10.1021/ja00232a057.

(102) Turlington, C. R.; Harrison, D. P.; White, P. S.; Brookhart, M.; Templeton, J. L. Probing the Oxidation Chemistry of Half-Sandwich Iridium Complexes with Oxygen Atom Transfer Reagents. *Inorg. Chem.* **2013**, *52* (19), 11351–11360. https://doi.org/10.1021/ic4016405.

(103) Sykes, A. G.; Mann, K. R. X-Ray Crystal Structure and Homonuclear 31P-31P δ/J-Resolved NMR Spectroscopic Studies of [AgIr2(Dimen)4(PPh3)2](PF6)3. Observation of a Statistical Mixture of "Head/Tail" Isomers. *Inorg. Chem.* **1990**, *29* (22), 4449–4453. https://doi.org/10.1021/ic00347a023.

(104) Einstein, F. W. B.; Jones, R. H.; Zhang,' And, X.; Sutton', D.; Zhang, X.; Sutton, D. *Synthesis and X-Ray Structure Determination of the Ir-Ag-Ir Donor-Acceptor Metal-Metal Bonded Complex [{(Q5-~5~e5)(~~),~r}~~g][~~4]*.

(105) Liston, D. J.; Reed, C. A.; Eigenbrot, C. W.; Scheidt, W. R. Donor-Acceptor Metal-Metal Bonding Instead of Metathesis With Vaska'S Compound and The Silver(i) Salt of The Weakly Coordinating Anion B11ch12-. *Inorganic Chemistry*. American Chemical Society August 1, 1987, pp 2739–2740. https://doi.org/10.1021/ic00264a002.

(106) Xie, Z.; Jelinek, T.; Bau, R.; Reed, C. A. New Weakly Coordinating Anions. III. Useful Silver and Trityl Salt Reagents of Carborane Anions. *J. Am. Chem. Soc.* **2002**, *116* (5), 1907–1913. https://doi.org/10.1021/JA00084A034.

(107) Qian, B.; Ward, D. L.; Smith, M. R. Synthesis, Structure, and Reactivity of β-Diketiminato Aluminum Complexes. *Organometallics* **1998**, *17* (14), 3070–3076. https://doi.org/10.1021/om970886o.

(108) Rivard, E.; Ragogna, P. J.; McWilliams, A. R.; Lough, A. J.; Manners, I. Reversible Skeletal Transmetalations of Inorganic Rings: Isolation of Aluminatophosphazenes, a Zwitterionic Phosphazene, and a Donor-Stabilized Alumazine-Phosphazene Hybrid Cation. *Inorg. Chem.* **2005**, *44* (19), 6789–6798. https://doi.org/10.1021/ic0509938.

(109) Butler, M. J.; Crimmin, M. R. Magnesium, Zinc, Aluminium and Gallium Hydride Complexes of the Transition Metals. *Chem. Commun.* **2017**, *53* (8), 1348–1365. https://doi.org/10.1039/c6cc05702k.

(110) Barron, A. R.; Wilkinson, G. Transition-Metal Aluminohydride Complexes. *Polyhedron* **1986**, *5* (12), 1897–1915. https://doi.org/10.1016/S0277-5387(00)87113-2.

(111) Riddlestone, I. M.; Abdalla, J. A. B.; Aldridge, S. Coordination and Activation of E-H Bonds (E=B, Al, Ga) at Transition Metal Centers. In *Advances in Organometallic Chemistry*; Academic Press, 2015; Vol. 63, pp 1–38. https://doi.org/10.1016/bs.adomc.2015.02.003.

TOC